Nuclear Science
NEA/NSC/DOC(2007)18

ISBN 978-92-64-99035-7

NUCLEAR SCIENCE COMMITTEE
COMMITTEE ON SAFETY OF NUCLEAR INSTALLATIONS

VVER-1000 Coolant Transient Benchmark

Phase I (V1000CT-1)

Volume 3: Summary Results of Exercise 2 on Coupled 3-D Kinetics/Core Thermal-hydraulics

Boyan D. Ivanov and Kostadin N. Ivanov
Nuclear Engineering Program
The Pennsylvania State University

NEA No. 6201

NUCLEAR ENERGY AGENCY
ORGANISATION FOR ECONOMIC CO-OPERATION AND DEVELOPMENT

ORGANISATION FOR ECONOMIC CO-OPERATION AND DEVELOPMENT

The OECD is a unique forum where the governments of 30 democracies work together to address the economic, social and environmental challenges of globalisation. The OECD is also at the forefront of efforts to understand and to help governments respond to new developments and concerns, such as corporate governance, the information economy and the challenges of an ageing population. The Organisation provides a setting where governments can compare policy experiences, seek answers to common problems, identify good practice and work to co-ordinate domestic and international policies.

The OECD member countries are: Australia, Austria, Belgium, Canada, the Czech Republic, Denmark, Finland, France, Germany, Greece, Hungary, Iceland, Ireland, Italy, Japan, Korea, Luxembourg, Mexico, the Netherlands, New Zealand, Norway, Poland, Portugal, the Slovak Republic, Spain, Sweden, Switzerland, Turkey, the United Kingdom and the United States. The Commission of the European Communities takes part in the work of the OECD.

OECD Publishing disseminates widely the results of the Organisation's statistics gathering and research on economic, social and environmental issues, as well as the conventions, guidelines and standards agreed by its members.

* * *

This work is published on the responsibility of the Secretary-General of the OECD. The opinions expressed and arguments employed herein do not necessarily reflect the official views of the Organisation or of the governments of its member countries.

NUCLEAR ENERGY AGENCY

The OECD Nuclear Energy Agency (NEA) was established on 1st February 1958 under the name of the OEEC European Nuclear Energy Agency. It received its present designation on 20th April 1972, when Japan became its first non-European full member. NEA membership today consists of 28 OECD member countries: Australia, Austria, Belgium, Canada, the Czech Republic, Denmark, Finland, France, Germany, Greece, Hungary, Iceland, Ireland, Italy, Japan, Luxembourg, Mexico, the Netherlands, Norway, Portugal, Republic of Korea, the Slovak Republic, Spain, Sweden, Switzerland, Turkey, the United Kingdom and the United States. The Commission of the European Communities also takes part in the work of the Agency.

The mission of the NEA is:

- to assist its member countries in maintaining and further developing, through international co-operation, the scientific, technological and legal bases required for a safe, environmentally friendly and economical use of nuclear energy for peaceful purposes, as well as
- to provide authoritative assessments and to forge common understandings on key issues, as input to government decisions on nuclear energy policy and to broader OECD policy analyses in areas such as energy and sustainable development.

Specific areas of competence of the NEA include safety and regulation of nuclear activities, radioactive waste management, radiological protection, nuclear science, economic and technical analyses of the nuclear fuel cycle, nuclear law and liability, and public information. The NEA Data Bank provides nuclear data and computer program services for participating countries.

In these and related tasks, the NEA works in close collaboration with the International Atomic Energy Agency in Vienna, with which it has a Co-operation Agreement, as well as with other international organisations in the nuclear field.

FOREWORD

The Nuclear Energy Agency (NEA) of the Organisation for Economic Co-operation and Development (OECD) has completed under United States Nuclear Regulatory Commission (NRC) sponsorship a PWR main steam line break (MSLB) benchmark against thermal-hydraulic/neutron kinetics codes. Recently, another OECD/NRC coupled code benchmark was completed for a BWR turbine trip (TT) transient. During the course of defining and co-ordinating the OECD/NRC PWR MSLB and BWR TT benchmarks, a systematic approach was established to validate best-estimate coupled codes. This approach employs a multi-level methodology, allowing for a consistent and comprehensive validation process. It also contributes to determining additional requirements that aid in the preparation of a basis for licensing applications of coupled calculations for a specific reactor type, i.e. to establish safety expertise in analysing reactivity transients. Professional communities were formed during the course of these benchmark activities that allowed in-depth discussions of different aspects of accessing neutron kinetics modelling for a given reactor and how to implement best-estimate methodologies for transient analysis using coupled codes. The above examples demonstrate the benefit of establishing such international coupled standard problems for each type of reactor.

In the framework of the United States Department of Energy (DOE) International Nuclear Safety Program (INSP) a project has been started with the overall objective to assess computer codes used in the safety analysis of VVER power plants, specifically for their use in analysing reactivity transients in a VVER-1000 reactor. As a result, a coupled benchmark problem based on data from the Bulgarian Kozloduy nuclear power plant was developed for the purpose of assessing neutron kinetics modelling for a VVER-1000 reactor. This problem is being analysed with both point kinetics and three-dimensional kinetics models. Based on the experience accumulated in safety analyses of Western-type reactors (see the above examples for PWR and BWR international standard benchmark problems), it was proposed that the VVER-1000 benchmark problem be extended to an international standard problem. At its topical meeting in Paris in June 2001, the NEA Nuclear Science Committee (NSC) endorsed this extension, resulting in the coupled VVER-1000 benchmark problem becoming an international standard problem for validation of the best-estimate safety codes for VVER applications.

During the Starter International VVER-1000 Benchmark Meeting, which took place in Dresden, Germany in May 2002, participants agreed to label the above-mentioned VVER-1000 benchmark as the VVER-1000 Coolant Transient Benchmark (V1000CT), consisting of two phases. Phase I (V1000CT-1), led by Pennsylvania State University (PSU), is a main coolant pump (MCP) switching-on transient while the three other MCP are in operation. Phase II (V1000CT-2), led by the *Commissariat à l'énergie atomique* (CEA), includes calculation of coolant mixing experiments and an MSLB analysis. Both PSU and the CEA are working in co-operation with the Institute for Nuclear Research and Nuclear Energy (INRNE). The sponsors of the benchmark are the OECD/NEA, the US DOE, the CEA and the *Institut de radioprotection et de sûreté nucléaire* (IRSN). The Kozloduy nuclear power plant (KNPP) provides technical support and the Atomic Energy Research (AER) Working Group D participates and collaborates in the benchmark activities.

The V1000CT-1 benchmark will be published in four volumes. The first volume, published in 2002, provides the specification for the V1000CT-1 benchmark problem. The report was prepared jointly by PSU (United States) and INRNE (Bulgaria), in co-operation with leading specialists from

the KNPP. The specification covers the three exercises of Phase I and describes the required output information for each exercise. In addition, a CD-ROM was prepared with the transient boundary conditions, decay heat values as function of time and cross-section libraries.

Volume 2, published in 2006, summarises the results for Exercise 1 of the benchmark and identifies the key parameters and important issues concerning the thermal-hydraulic system modelling of the simulated transient. Exercise 1 helped the participants to initialise and test their system code models for further use in Exercise 3 on coupled 3-D kinetics/system thermal-hydraulics simulations.

Volume 3 summarises the results for Exercise 2 of the benchmark and identifies the key parameters and important issues concerning the 3-D neutron kinetics modelling of the simulated transient. Exercise 2 helped the participants to initialise and test their coupled 3-D neutron kinetics core thermal-hydraulics boundary conditions models for further use in Exercise 3 on coupled 3-D kinetics/ system thermal-hydraulics simulations. This report is supplemented with brief descriptions of the coupled codes used (for modelling core neutronics and thermal-hydraulics) as provided by the participants (Appendix A). Descriptions of the models used are also given (Appendix B). The latter are presented as answers to the questionnaire for Exercise 2 so that compliance with the specification can be verified. Appendices C and D are only provided in the CD-ROM version of the report, available on request. Appendix C contains the mean solutions for each type of data and the parameters generated using the statistical methodology developed at PSU. These solutions are used as reference results for code-to-code comparisons with the participants' results. The participants' deviations and figures of merit for each parameter are presented in Appendix D. Readers are invited to note that many of the figures in the report are in colour. Colour versions of the figures are available in the online version of the report on the NEA website (www.nea.fr).

Volume IV, which will summarise the results for Exercise 3 on coupled 3-D kinetics/system thermal-hydraulics simulations, is the final report of the V1000CT-1 benchmark and is due to be published in 2008.

Acknowledgements

The authors would like to thank Dr. J. Roglans-Ribas, Dr. T. Taiwo, Dr. P. Pizzica, and J. Ahrens from the Argonne National Laboratory (ANL), whose support and encouragement in establishing and carrying out this benchmark are invaluable.

This report is the sum of many efforts, the participants, the funding agencies and their staff – the US Department of Energy, CEA and the Organisation of Economic Co-operation and Development. Special appreciation goes to the report reviewers: S. Langenbuch from Gesellschaft für Anlagen- und Reaktorsicherheit (GRS), P. Siltanen from Fortum Nuclear Services Ltd, and J.M. Aragones from Universidad Politecnica Madrid (UPM). Their comments and suggestions were very valuable and significantly improved the quality of this report.

The authors wish to express their sincere appreciation for the outstanding support offered by the KNPP personnel in providing the plant data and discussing the transient characteristics.

The authors would like to thank Prof. J. Aragones from UPM – member of NSC /NEA and Prof. F. D'Auria of University of Pisa (UPISA) – member of CSNI/NEA, whose support and encouragement in establishing and carrying out this benchmark are invaluable.

The authors wish to express their sincere appreciation for the outstanding support offered by Dr. Enrico Sartori, who not only provided efficient administration, organisation and valuable technical recommendations, but most importantly provided friendly counsel and advice.

Finally, we are grateful to Amanda Costa and Roopa Chauhan for having devoted their competence and skill to the final editing of this report.

TABLE OF CONTENTS

Appendices C and D available on CD-ROM

List of tables

List of figures

LIST OF ABBREVIATIONS

1-D	One-dimensional
2-D	Two-dimensional
3-D	Three-dimensional
ACAP	Automated Code Assessment Program
ADF	Assembly discontinuity factor
AER	Atomic energy research
AFEN	Analytic Function Expansion Nodal Method
ANL	Argonne National Laboratory
AO	Axial offset
APF	Axial peaking factor
ARI	All rods in
ARO	All rods out
BC	Boundary condition
BOC	Beginning of cycle
BWR	Boiling water reactor
CEA	Commissariat à l'Énergie Atomique
CGR	Coarse group rebalance
CR	Control rod
CT	Coolant transient
DF	Discontinuity factor
DOE	Department of Energy
EFPD	Effective full power days
EHTC	Electro-hydraulic turbine controller
ERW	Ejected rod worth
FA	Fuel assembly
FEM	Finite Element Method
FOM	Figure of merit
FZK	Forschungszentrum Karlsruhe
FZR	Forschungszentrum Rossendorf
GRS	Gesellschaft für Anlagen- und Reaktorsicherheit
HP	Hot power
HZP	Hot zero power
INRNE	Institute for Nuclear Research and Nuclear Energy

INSP	International Nuclear Safety Program
KAIST	Korea Advanced Institute of Science and Technology
KNPP	Kozloduy nuclear power plant
KU	Kiev University
LWR	Light water reactor
MCP	Main coolant pump
ME	Mean error
MSE	Mean square error
MSLB	Main steam line break
NEA	Nuclear Energy Agency
NEM	Nodal Expansion Method
NPP	Nuclear power plant
NRC	Nuclear Regulatory Commission
NRI	Nuclear Research Institute
NRS	Nuclear reactor system
NSC	Nuclear Science Committee
OECD	Organisation for Economic Co-operation and Development
PSU	Pennsylvania State University
PWR	Pressurised water reactor
RCS	Reactor coolant system
RPF	Radial peaking factor
SDRS	Soviet-designed Reactor Safety
SG	Steam generator
TG	Turbo generator
TPEN	Triangular Polynomial Expansion Nodal Method
TRW	Tripped rod worth
TT	Turbine trip
UPISA	University of Pisa
UPM	Universidad Politecnica Madrid
V1000CT	VVER-1000 Coolant Transient
VTT	Valtion Teknillinen Tutkimuskeskus
VVER	Water water power reactor

Chapter 1

INTRODUCTION

In the past, analysis of plant transients and of the reactor core behaviour were performed separately. Usually, the core was represented by a point kinetics model to analyse plant transients, and for the core calculations, boundary conditions were imposed at the inlet and the outlet of the core. In reality, these boundary conditions depend on the power generation in the core. To ensure a realistic description of the physical phenomena in an accident analysis the application of the coupled codes is required.

In recent years code developers started coupling three-dimensional (3-D) neutron kinetics codes with advanced thermal-hydraulics system codes. Such complex computer codes allow modelling of the entire reactor system including a 3-D neutronics core. When one analyses reactivity initiated accidents with an asymmetric neutron flux distribution in the core, only such coupled codes are capable of estimating the real feedback effects. These codes can perform safety analyses in order to replace the conservative estimations with best-estimate calculations.

The US Department of Energy has established a national laboratory team to support the planning, management and implementation of its Soviet-Designed Reactor Safety Program (SDRS). One of the goals of this programme is to develop models for VVER reactors for use in coupled thermal-hydraulics/ neutron kinetics codes for analysis of specific transients. The specific technical goals of the project are:

- development of the methodology of performing coupled thermal-hydraulics/neutron kinetics multi-dimensional analyses of VVER reactors;

- development and analysis of benchmark problems to determine applicability of the three-dimensional coupled thermal-hydraulics/neutron kinetics codes to safety analysis of VVER special transients.

As a result, a benchmark problem has been established in order to determine the applicability of the coupled codes to safety analysis of VVER special transients [1]. A small benchmark team at PSU was responsible for authoring the VVER-1000 benchmark specification based on Bulgarian Kozloduy NPP data. Based on the experience of the PSU team accumulated in safety analyses of the Western-type reactors (PWR MSLB [2] and BWR TT [3]) it was proposed that the VVER-1000 benchmark problem be extended to an international standard problem. At its topical meeting in Paris (June 2001) the Nuclear Science Committee of the OECD/NEA approved and endorsed the developed coupled VVER-1000 benchmark problem as an international standard problem for validation of the best-estimate safety codes for VVER applications, which they labelled as the V1000CT Benchmark.

The V1000CT-1 Benchmark Specification [4] was prepared jointly by PSU and INRNE in co-operation with leading specialists from the Kozloduy NPP. The reference problem chosen for simulation in a VVER-1000 is one main coolant pump (MCP) switching on while the other three MCPs are in operation. It is an experiment that was conducted by Bulgarian and Russian engineers during the plant-commissioning phase at the KNPP Unit #6 as a part of the start-up tests. The test was

carried out due to its importance for the safety of the NPP with VVER-1000, model 320. This event is characterised by a rapid increase in flow through the core resulting in a coolant temperature decrease, which is spatially dependent.

The V1000CT-1 benchmark has three main goals: to verify the capability of system codes to analyse complex transients with coupled core-plant interactions; to fully test the 3-D neutronics/ thermal-hydraulic coupling; to evaluate discrepancies between predictions of coupled codes in best-estimate transient simulations and between coupled codes predictions and plant data.

The three exercises discussed below fulfil the goals of this benchmark:

- *Exercise 1 – Point kinetics plant simulation.* The purpose of this exercise is to test the primary and secondary system model responses using a point kinetics simulation. The benchmark specification provides all the necessary point kinetics data. Using this exercise the participants can verify their input decks and they can eliminate all the problems coming from the user modelling, which later could be helpful for the best-estimate comparisons.

- *Exercise 2 – Coupled 3-D neutronics/core thermal-hydraulics response evaluation.* The purpose of this exercise is to model the core and the vessel only. The benchmark provides inlet and outlet core transient boundary conditions. Using this exercise the participants can verify their coupling schemes and cross-section library utilisation, and they can improve their input decks.

- *Exercise 3 – Best-estimate coupled code plant transient modelling.* The first two exercises are preparation for the third exercise. The third exercise combines elements of the first two. In this exercise the participants must analyse the transient in its entirety.

This report summarises the comparative analyses of the submitted results for Exercise 2. In total, 10 results were submitted by participants representing 9 organisations from 8 countries. Table 1.1 shows the list of participants in Exercise 2 and the code names used for the simulation.

Table 1.1. List of participants in Exercise 2

Participant number	Company name	Country	Code
1	CEA	France	CRONOS2/FLICA4
2	FZK	Germany	RELAP5/PARCS
3	FZR	Germany	DYN3D
4	KAIST	Korea	COREDAX
5	KU	Ukraine	RELAP5-3D
6	NRI-1	Czech Republic	DYN3D Version 3.1
7	NRI-2	Czech Republic	DYN3D Version 3.2
8	PSU	USA	TRAC-PF1/NEM
9	UPISA	Italy	RELAP5/PARCS
10	VTT	Finland	HEXTRAN

Chapter 2 gives a brief review of the benchmark specifications relevant to Exercise 2. Chapter 3 discusses the comparative statistical methodology utilised for integral parameters, 1-D values, 2-D values and time histories. Chapter 4 provides the comparative analysis of the final results of Exercise 2 and Chapter 5 describes in-depth analysis of the observed deviations. Chapter 6 gives a brief summary of the conclusions drawn from the analysis of Exercise 2.

Chapter 2

REVIEW OF EXERCISE 2

2.1 Introduction

In the first benchmark exercise the participants initialised their system models and tested the thermal-hydraulic system responses using specified point kinetics parameters. The purpose of Exercise 2 of the V1000CT-1 benchmark is to test the core neutronics response to imposed thermal-hydraulic boundary conditions and to initialise the participants' coupled 3-D core models. Completing the first two benchmark exercises will allow for a thorough examination of the coupled core/plant system transient modelling in Exercise 3 using the models developed in the first and second exercises.

The purpose of the second exercise is to model the core and the vessel only. Inlet and outlet core transient boundary conditions are provided. The boundary conditions [core inlet mass-flow rate (MFR) distribution, core inlet temperature distribution and core outlet pressure distribution] were obtained by the benchmark team using the TRAC-PF1/NEM coupled code. The boundary conditions can be downloaded from the benchmark ftp site.

The reference design for the VVER-1000 is derived from the reactor geometry and operational data of Kozloduy NPP Unit #6. The data provided in the benchmark specifications, appendices and in the relevant tables and figures completely defines the VVER-1000 benchmark exercise [4].

During the plant commissioning phase at Kozloduy NPP Unit #6 a number of experiments were performed. One of the experiments investigated the behaviour of the nuclear power reactor parameters in case of switching-on one main coolant pump while the other three main coolant pumps remain in operation. The experiment's goal was a thorough test of the reliability of all power plant equipment.

Before the experiment, the reactor power level was reduced from 75% of the nominal level (2 250 MW) to approximately 21% by consecutive switching-off of MCP #2 and MCP #3. A few hours before the experiment MCP #2 was switched back on, and the power was stabilised at 30% following the technical specification requirements. According to the technical specification for safety operation of Units #5 and #6 (both VVER-1000), switching on one main coolant pump in operation is performed when the reactor power is at 30% of the nominal level.

During the experiment in which MCP #3 was switched on, the system and equipment of Unit #6 performed according to the design requirements for the corresponding level of reactor power. Design equipment registers and records the parameters in case of a transient event.

At the beginning of the transient the initial power level is about 30% of the nominal with control rod group #10 being 36% withdrawn from the reactor core. Analysis of the initial 3-D relative power distribution showed that this insertion introduced axial neutronic asymmetry in the core. At the beginning of the transient a thermal-hydraulic asymmetry coming from the colder water introduced into one quarter of the core when MCP #3 is switched on is observed. The sector of colder water introduces positive reactivity into the core in an asymmetric manner.

2.2 Initial steady-state conditions

The reactor is at the beginning of the cycle (BOC) with an average core exposure of 30.7 Effective Full Power Days (EFPD) and boron concentration of 5.95 g/kgH_2O. The experiment begins with three pumps in operation (1st, 2nd and 4th) and, according to the equipment that controls neutron flux, reactor power is at 27.45% of nominal power level. MCP #1, #2 and #4 are working under stable conditions and MCP #3 is out of operation. Table 2.1 lists the initial conditions. The inlet temperature in the reactor core is about 555.00 K. The temperature differences, between the hot and cold legs for the loop with working MCP, vary between 8.3 and 11.5 K while the same temperature difference for loop #3, with the MCP out of operation, is -3.6 K. The total mass flow through the core is about 13 611 kg/s with an average flow of 5 000 kg/s through each of the working loops and negative (reverse) flow of –1 544 kg/s in loop #3. The Electro-Hydraulic Regulative System supports the pressure in the main steam collector when the Turbine Generator works at 164.0 ± 10 MW. All regulators are in the automatic regime. Table 2.2 shows initial steady state definitions. The initial conditions of the transient described above are referred to as Hot Power (HP) conditions. Additionally, we define a Hot Zero Power (HZP) state for initialisation of the 3-D core neutronics model for the second exercise. The HZP conditions are defined as follows: the power level is 0.1% of the nominal power; the uniform spatial fuel temperature is 552.15 K and the moderator density is 767.1 kg/m^3.

Table 2.1. Initial conditions for KNPP Unit 6

Parameter	Value
Core power, MWt	824.00
Primary side pressure, MPa	15.6
RCS first cold leg temperature, K	555.55
RCS second cold leg temperature, K	554.55
RCS third cold leg temperature, K	554.35
RCS fourth cold leg temperature, K	555.25
RCS first hot leg temperature, K	567.05
RCS second hot leg temperature, K	562.85
RCS third hot leg temperature, K	550.75
RCS fourth hot leg temperature, K	566.15
Core flow rate, kg/s	13 611
First loop flow rate, kg/s	5 031
Second loop flow rate, kg/s	5 069
Third loop flow rate, kg/s	-1 544
Fourth loop flow rate, kg/s	5 075
Pressuriser level, m	7.44
Water level in SG1, m	2.30
Water level in SG2, m	2.41
Water level in SG3, m	2.49
Water level in SG4, m	2.43
Secondary side pressure, MPa	5.937

Table 2.2. Definition of steady states

Number	T-H conditions	Control rod positions
0	HZP	Groups 1-8 ARO[1] Group 9 is 36% inserted Groups 10 ARI[2]
1	HP	Groups 1-9 ARO Group 10 is 36% withdrawn

[1]ARO – all rods out
[2]ARI – all rods inserted

2.3 Transient calculations

The transient test scenario is as follows:

1) At reactor power 27.45% N_{nom} MCP #3 is switched on.

2) After switching on MCP #3 the reactor power gradually increases to 29.8% N_{nom}.

3) Pressuriser water level decreases from 744 cm to 728 cm.

4) Water level in steam generator #3 decreases by 9 cm.

5) EHTC supports the pressure in MSH at a level of 6.0 ± 0.05 MPa when the TG power is 164.0 ± 10 MW.

6) The flow rate in loop #3 reverses back to normal at the 13 seconds after the switching-on of MCP #3. The timing is consistent with the increase in reactivity, as observed by the reactor power set points.

During the transient there is an increased mass flow through the core because MCP #3 is switched on. The cooling of the core is improved and redistributed while the thermal core power level increases slightly (the total power increase during the transient is between 27.46% and 29.8% of the nominal level). The non-symmetric cooling of the reactor core results in non-symmetric reactivity feedback and subsequently non-symmetric radial power distribution.

The transient ends with a temperature difference between the hot and cold legs of loops #1, #2 and #4 slightly decreases:

- for loop #1 – from 11.5 K to 8.8 K;
- for loop #2 – from 8.3 K to 8.4 K;
- for loop #4 – from 10.9 K to 8.9 K;
- for loop #3 – from -3.6 K to 8.2 K.

The most noticeable change is in the temperature difference for loop #3. This results in a dynamically changing spatial distribution of reactivity feedback during the transient and subsequently in a dynamically changing spatial power distribution.

Chapter 3

STATISTICAL METHODOLOGY AND DATA PROCESSING

This chapter presents the statistical methodology used for the comparative analysis of the results for Exercise 2 of the V1000CT-1 benchmark. As mentioned earlier, 10 sets of results were submitted to the benchmark team. These results consist of integral parameters, 1-D and 2-D distributions, and time histories. The time histories had to be processed in order to be compared. The following subsections describe the statistical methodology used in analysing the different results and the data processing involved.

3.1 Integral parameters

The integral parameters include most of the initial steady-state values. Since plant measured data does not exist for all of the required integral parameters, the mean value has been calculated and participants' results have been compared to it. Mean value, standard deviation, deviation and figure of merit (FOM) are calculated according to Eqs. (3.1-3.4) respectively:

$$x_{reference} = \frac{\sum_{i}^{N} x_i}{N} \tag{3.1}$$

$$\sigma = \pm\sqrt{\frac{\sum \left(x_i - x_{reference}\right)^2}{N-1}} \tag{3.2}$$

where σ is the standard deviation, x_i is the data submitted by each participant and N is the total number of received results.

The deviation and FOM can be computed as:

$$e_i = x_i - x_{reference} \tag{3.3}$$

$$\Phi_i = \frac{e_i}{\sigma} \tag{3.4}$$

where e_i is the difference between the participant's value and the mean value. The Φ_i closer to zero indicates that participant results are closer to the reference solution.

3.2 One-dimensional axial distributions

Exercise 2 contains steady-state snapshots of core average axial power distribution as a function of height or number of axial nodes. The axial power distribution can be displayed as an x-y plot.

Similar methods of statistical analysis as those described in the previous section can be applied for each axial cell. Analyses are performed for each 1-D cell according to the Eqs. (3.1-3.4). A table was prepared that shows the deviations from mean and FOM at each axial position for each participant.

3.3 Two-dimensional radial distributions

Exercise 2 also contains steady-state and transient snapshots of the radial distribution through the core for certain parameters. Due to the two-dimensional nature of such data, it is difficult to plot the results; this is not the case with time history data and 1-D distributions. However, the same statistical methods can be used to generate mean values, standard deviations, participant deviations and FOMs.

Mean and standard deviation for each 2-D cell can be computed according to Eqs. (3.1) and (3.2). Such an analysis results in a 2-D map for mean values and standard deviations, rather than a single value for each parameter. Comparisons can therefore be made for each cell, not only for specific cells of interest.

The deviation and FOM can be computed according to Eqs. (3.3) and (3.4), respectively. For each participant, a map is generated that shows deviations from the mean and the FOM at each radial position.

3.4 Time histories

Five different sets of time histories were submitted by the participants for which plant measured data does not exist. The mean value was used as a reference in the statistical processing described in the next subsection. The time histories are compared in plots and FOM was calculated using the Automated Code Assessment Program (ACAP) [5].

3.5 ACAP

The comparative analyses were performed for code-to-code comparisons using the standard statistical methodology with the ACAP [5]. ACAP is a tool developed to provide quantitative comparisons between nuclear reactor systems code results and experimental measurements. This software was developed at PSU under NRC contract for use in PSU's code consolidation efforts. ACAP's capabilities are described as follows:

- draws upon a mathematical toolkit to compare experimental data and NRS code simulations;
- returns quantitative FOM associated with individual and suite comparisons;
- accommodates the multiple data types encountered in NRS environments;
- incorporates experimental uncertainty in the assessment;
- provides "event windowing" capability;
- accommodates inconsistencies between measured and computed independent variables (e.g. different time steps);
- provides a framework for automated, tunable weighting of component measures in the construction of overall FOM accuracy.

ACAP is a PC- and UNIX-station-based application that can be run interactively on PCs with Windows 95/98/NT, in batch mode on PCs as a WINDOWS console application or in batch mode on UNIX stations as a command line executable.

The Mean Error (ME), the Variance of Error (VE), the Mean Square Error (MSE) methods and their combination (normalised weight) were used for the FOM calculations for the time histories [5]. Figure 3.1 shows a snapshot of the FOM configuration in ACAP calculations for Exercise 2 of the benchmark. These methods are advanced techniques for analysis of time history data. The following equations represent the theory portion of these methods.

Figure 3.1. FOM configuration in ACAP

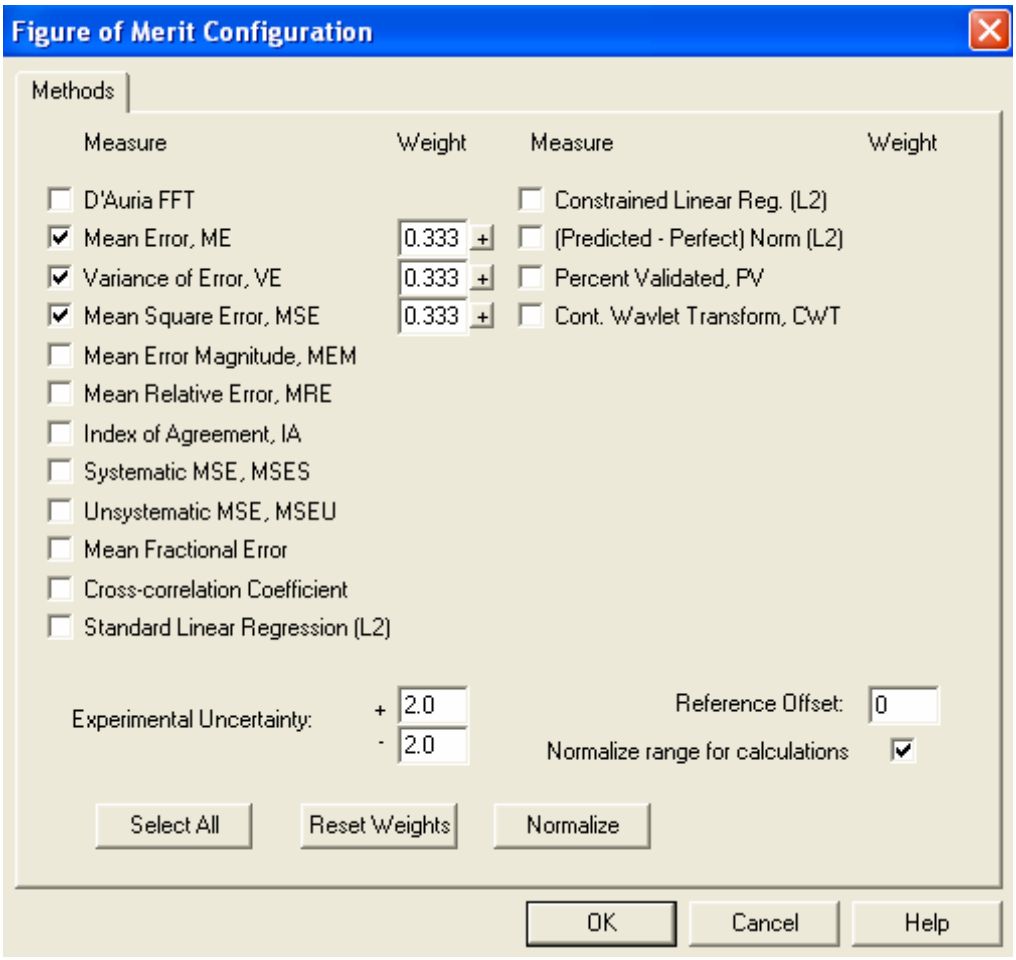

Mean Error (ME)

$$ME = \frac{1}{N}\left\{\sum_{i=1}^{N}(O_i - P_i)\right\} \tag{3.5}$$

where N is number of data values, i is the sample index, O_i is the i-th datum in experimental set P_i is the i-th datum in computed set.

Variance of Error (VE)

$$\sigma^2 = VE = \frac{1}{(N-1)}\left\{\sum_{i=1}^{N}(O_i - P_i - ME)^2\right\} \tag{3.6}$$

Mean Square Error (MSE)

$$MSE = \frac{1}{N}\left\{\sum_{i=1}^{N}(O_i - P_i)^2\right\} \tag{3.7}$$

The FOM equations for the three methods are outlined below:

$$FOM_{ME} = \frac{1}{(|ME|+1)} \tag{3.8}$$

$$FOM_{VE} = \frac{1}{(VE+1)} \tag{3.9}$$

$$FOM_{MSE} = \frac{1}{(MSE+1)} \tag{3.10}$$

FOM indicates that a participant result is closer to the reference solution if the FOM is closer to unity to indicate better agreement.

3.6 Data processing

The time-dependent participants' results had to be processed in order to be compared to each other. In order to avoid the effects of participants' initialisation for the initial steady state on the comparative analysis of transient results, the actual values of the time history data were replaced with *delta changes*. The delta changes were calculated by subtraction of initial value (at time zero) from the rest of the values of the time-history data.

Chapter 4

RESULTS AND DISCUSSION

4.1 Introduction

This chapter presents the comparative analyses of the results for Exercise 2 of Phase I of the VVER-1000 Coolant Transient Benchmark (V1000CT-1). The tables and figures in this chapter provide a comparison of the participants' results to the reference solution. The analyses of these results are grouped into three sections. In Section 4.2 we discuss the hot zero power (HZP) results. Section 4.3 presents steady-state results at the initial conditions and Section 4.4 presents the analyses of the transient results. Selected results are shown in this chapter, while the complete detailed comparison of the participants' results is provided in Appendix D (divided into four parts: D.1 – Integral parameters, D.2 – One-dimensional axial distributions, D.3 – Two-dimensional radial distributions and D.4 – Core averaged time evaluations).

Table 4.1 shows participants' models used for simulation of Exercise 2. This table provides information not only about the general nodalisation but also information for the utilisation of the boundary conditions provided in the specification: core inlet mass flow rate (MFR) distribution, core inlet temperature distribution and core outlet pressure distribution. This table, along with the answers to the questionnaire given in Appendix B, provide a good basis for analyses of the participants' results.

Table 4.1. Participants' models

Name	Country	Code	Boundary conditions			Core axial layers	Core T-H channels
			Inlet MFR	Inlet T	Outlet P		
CEA	France	CRONOS2/FLICA4	Yes	Yes	Yes	12	217
FZK	Germany	RELAP5/PARCS	Yes	Yes	Yes	10	18
FZR	Germany	DYN3D	Yes	Yes	Yes	12	24
KAIST	Korea	COREDAX	Yes	Yes	No	12	163
KU	Ukraine	RELAP5-3D	Yes	Yes	Yes	10	48
NRI-1	Czech Republic	DYN3D Version 3.1	Yes	Yes	Yes	12	24
NRI-2	Czech Republic	DYN3D Version 3.2	Yes	Yes	Yes	12	211
PSU	USA	TRAC-PF1/NEM	Yes	Yes	Yes	12	24
UPISA	Italy	RELAP5/PARCS	Yes	Yes	Yes	20	28
VTT	Finland	HEXTRAN	Yes	Yes	Yes	20	163

4.2 Hot zero power results

Hot zero power (HZP) state is not a real case and it is defined for initialisation of the 3-D core neutronics model. In this case, thermal-hydraulic feedback has been fixed so that the thermal-hydraulic core model does not play a role in these calculations. The HZP conditions are defined as follows: the

power level is 0.1% of the nominal power; the fuel temperature is 552.15 K and the moderator density is 767.1 kg/m^3. Control rod groups 1 to 8 are all rods out (ARO), control rod group 9 is 36% inserted into the core, and control rod group 10 is all rods in (ARI).

Figure 4.1 presents the comparison of the k_{eff} while Table 4.2 lists the deviation and FOM for each of the participants from the mean k_{eff}. Except for the KU and PSU results, the rest of the participants show reasonable agreement within 1σ. The significant difference of KU and PSU results from the rest of the results will also be observed for most of the parameters that will be compared in this chapter. This difference is analysed in depth in the next chapter. Summarising the conclusions from the next chapter, this difference is mostly due to the difference in the methods used in the different codes for solving the diffusion equation in hexagonal geometry.

Figure 4.2 presents the comparison of the radial peaking factor (RPF) while Table 4.3 lists the deviation and FOM for each of the participants from the mean RPF. Again it can be seen that the KU and PSU results differ significantly from the rest of the results. All the participants' results, except KU and PSU, are within 1σ.

Figure 4.3 shows the comparison of the axial peaking factor (APF) while Table 4.4 gives the deviation and FOM for each of the participants from the mean APF. It can be observed that the results of UPISA and VTT significantly deviate from the rest of the results. These results show the importance of the axial nodalisation of the core. UPISA and VTT use 20 axial layers in the core (Table 4.1) while the other participants use a smaller number of axial layers. Overall reasonable agreement between the different codes can be observed from the presented results.

Figure 4.4 shows the comparison of the axial offset (AO) while Table 4.5 gives the deviation and FOM for each of the participants from the mean AO. The only result which significantly deviates from the mean is the VTT result. The reason for this deviation is most likely the modelling of the reflector. Instead of modelling the reflector with the provided cross-sections, the reflector was represented by using albedo boundary conditions, as reported in the VTT questionnaire.

Figures 4.5-6 and Tables 4.6-7 present the results, the deviation and the FOM for the ejected rod worth (ERW) and control rod group #10 worth (CR 10 W) respectively, for each of the participants. From these figures and tables it can be observed that the ERW and CR10 W predictions of PSU and KU again differ from the mean due to the reasons mentioned above. It is interesting to note that the FZK results for ERW are also significantly different from the rest of the results.

The tripped rod worth (TRW) results are shown in Figure 4.7 and Table 4.8. A comparison of these results shows that only VTT significantly deviate from the mean. However, it can be also noted that FZK and UPISA predict slightly higher tripped rod worth. This difference can be attributed to the fact that both organisations use the same 3-D neutronics code PARCS and, therefore, obtain similar results even though they use different nodalisation. It is likely that the PARCS code treats the CR insertion differently in comparison to the other codes.

Figure 4.8 and Tables 4.9-4.10 present the results for axial power distribution. Reasonable agreement between the participants' results can be observed. Only VTT results deviate from the mean due to the utilised reflector model, which has already been discussed.

A complete set of the reference results is provided in Appendix C and a complete set of the deviations of the submitted results for each of the participants is provided in Appendix D. The deviations of the 2-D normalised power distribution provided in Appendix D.3 again show significant deviation of KU and PSU results from the reference (mean) solution. The results of all participants are

within 1σ, while KU and PSU results are within 2σ. If the KU and PSU results are to be excluded from the mean calculation, this difference will become even more pronounced. As mentioned earlier, in-depth analyses of these deviations are provided in Chapter 5 of this report.

4.3 Hot power steady-state results

The benchmark specification defines hot power steady state (HP-SS) as a state immediately before the transient begins. The HP steady-state conditions are as follows:

- Reactor power is 824.0 MW.
- Control rod groups 1-9 are ARO.
- Control rod group 10 is 36% withdrawn from the core.
- Core inlet and outlet boundary conditions are used.

The HP-SS results show similar differences to the ones observed in the HZP results but in this case the differences for some of the parameters are more pronounced since the thermal-hydraulic feedback is no longer fixed. For example, from the k_{eff} comparison, shown in Figure 4.9 and Table 4.11, it can be seen that the KU and PSU results still deviate from the results of the rest of the participants. Surprisingly, however, for HP-SS the CEA results also significantly deviate from the mean while such deviation was not observed for the HZP case. The reason for this deviation could be the interpretation of the provided boundary conditions or the core thermal-hydraulic model.

Figure 4.10 presents the comparison of the radial peaking factor (RPF), while Table 4.12 lists the deviation and FOM for each of the participants from the mean RPF. In contrast to the HZP state KU and PSU results deviate not only from the rest of the participants' results but also between themselves. This difference is most likely due to the different number of TH channels used by these participants, as reported in Table 4.1.

Figure 4.11 shows the comparison of the axial peaking factor (APF) while Table 4.13 gives the deviation and FOM for each of the participants from the mean APF. Similarly to the HZP state, the results of UPISA and VTT significantly deviate from the rest of the results due to the more detailed axial nodalisation. CEA results also deviate significantly from the mean, which is not surprising given the k_{eff} comparison.

Figure 4.12 shows the comparison of the axial offset (AO) while Table 4.14 gives the deviation and FOM for each of the participants from the mean AO. These results show that CEA over-predicts the AO while PSU under-predicts the AO and the differences from the mean for the rest of the participants are within 1σ.

Figure 4.13 and Tables 4.15-4.16 present the results for axial power distribution. Reasonable agreement between the participants' results can be observed. However, it can be seen that CEA, KU, PSU and VTT results deviate from the mean with more than 1σ.

The comparison of the 2-D distributions of normalised power, core inlet moderator temperature, core inlet mass flow rate, core outlet moderator temperature, core outlet mass flow rate, core outlet moderator density, and Doppler temperature to the mean (provided in Appendix C) is shown for each participant in Appendix D.3. These comparisons generally show good agreement within 1σ for most

of the results. However, the deviations for some of the results exceed 2σ. The reasons for these differences can mostly be attributed to the different participant TH nodalisation as reported in Table 4.1. The differences at the core outlet are probably due to the fact that some of the participants used 3-D thermal-hydraulics models while others used multi-channel models consisting of 1-D parallel channels. The differences in the 2-D normalised radial power distribution remain in the same range as in the HZP state.

4.4 Transient results

The transient calculation was performed according to the following conditions:

- Initial reactor power is 824.0 MW.
- Control rod groups 1-9 are ARO.
- Control rod group 10 is 36% inserted into the core and does not move during the calculations.
- Core inlet and outlet transient boundary conditions were used.

Figures 4.14 and 4.18 show the comparison of the RPF at 15 seconds and 800 seconds respectively. Tables 4.17 and 4.22 list the deviation and FOM for each of the participants from the mean RPF. The 15th second is associated with the full reverse of the flow of loop #3, while the 800th second is the end of the transient. From these figures and tables, it can be seen that the trend of the difference remains the same as the HP steady-state case. Similar observations can be made for the APF (Figures 4.15 and 4.19, Tables 4.18 and 4.23), the AO (Figures 4.16 and 4.20, Tables 4.19 and 4.24) and the axial power distribution (Figures 4.17 and 4.21, Tables 4.20-4.21 and 4.25-4.26).

The time history of the reactor power level predicted by the participants is shown in Figure 4.22. The initial reactor power and the FOM for each of the participants are provided in Table 4.27. The reactor power predicted by all of the participants has the same initial value and all participants' predictions also show fairly good agreement at the end of the transient. However, the power trend predicted by CEA, PSU and FZR differs from the trend predicted by rest of the participants. Similar to Exercise 1, this difference is caused by the use of different heat-structure models. At PSU, the gas gap conductance is a fixed value, while most of the participants use dynamical gas gap conductance modelling. This difference in the gas gap conductance model also reflects the observed differences in the fission power (Figure 4.23), the core average fuel temperature (Figure 4.24) and the maximum nodal average fuel temperature (Figure 4.26). Another reason for the differences in the PSU results could be the model of the fuel rod. In TRAC-PF1 an annular fuel pellet is impossible to model explicitly.

Figure 4.25 shows a reasonably good agreement of the core average moderator density between the participants except the CEA prediction, which shows significantly lower moderator density in comparison to the rest of the participants' results. As mentioned earlier, the reason for the deviation in the CEA results could be how the provided boundary conditions or the core thermal-hydraulic model are interpreted.

The comparison of the predicted 2-D distributions of normalised power, core inlet moderator temperature, core inlet mass flow rate, core outlet moderator temperature, core outlet mass flow rate, core outlet moderator density and Doppler temperature to the mean solutions (provided in Appendix C) at 15 seconds and 800 seconds is shown for each participant in Appendix D.3. These comparisons generally show good agreement within 1σ for most of the results. However, the deviations for some of

the results exceed 2σ. The reasons for these differences can mostly be attributed to the different participant TH nodalisations as reported in Table 4.1 and the utilisation of the provided boundary conditions. The differences at the core outlet are probably due to the fact that some of the participants used 3-D models, while others used 1-D channels. The differences in the 2-D normalised radial power distribution at 15 seconds and 800 seconds remain in the same range as in the HZP and HP-SS states.

Figure 4.1. HZP k_{eff} comparison

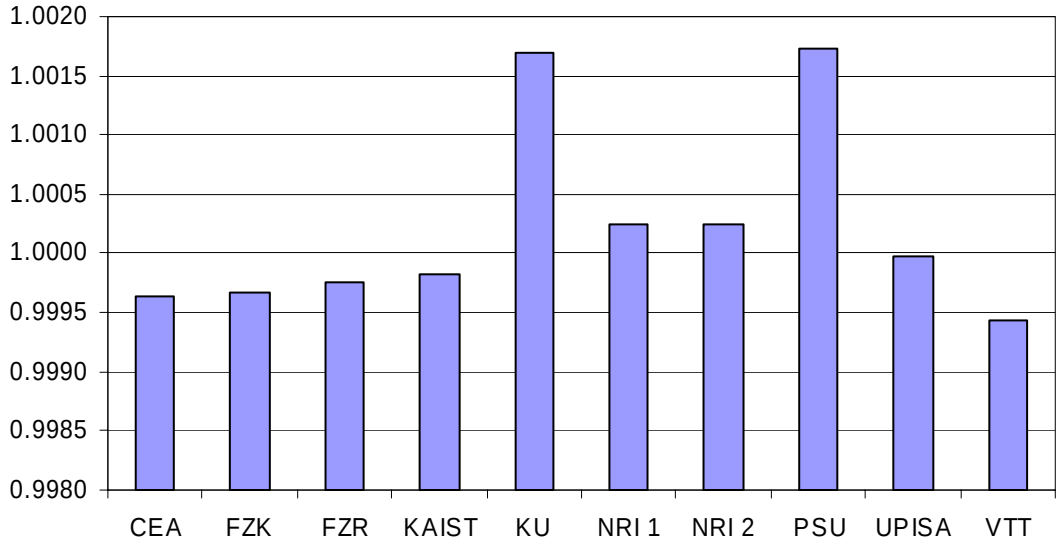

Table 4.2. Participant deviations and figure of merit for HZP k_{eff}

Participant	k_{eff}	Deviation	FOM
CEA	0.99963	-0.00059	-0.71
FZK	0.99967	-0.00055	-0.67
FZR	0.99975	-0.00047	-0.57
KAIST	0.99982	-0.00040	-0.48
KU	1.00169	0.00147	1.78
NRI 1	1.00025	0.00003	0.03
NRI 2	1.00025	0.00003	0.03
PSU	1.00173	0.00151	1.83
UPISA	0.99997	-0.00025	-0.30
VTT	0.99944	-0.00078	-0.94
Mean	1.00022	–	–
Standard deviation	0.00083	–	–

Figure 4.2. HZP radial peaking factor (RPF) comparison

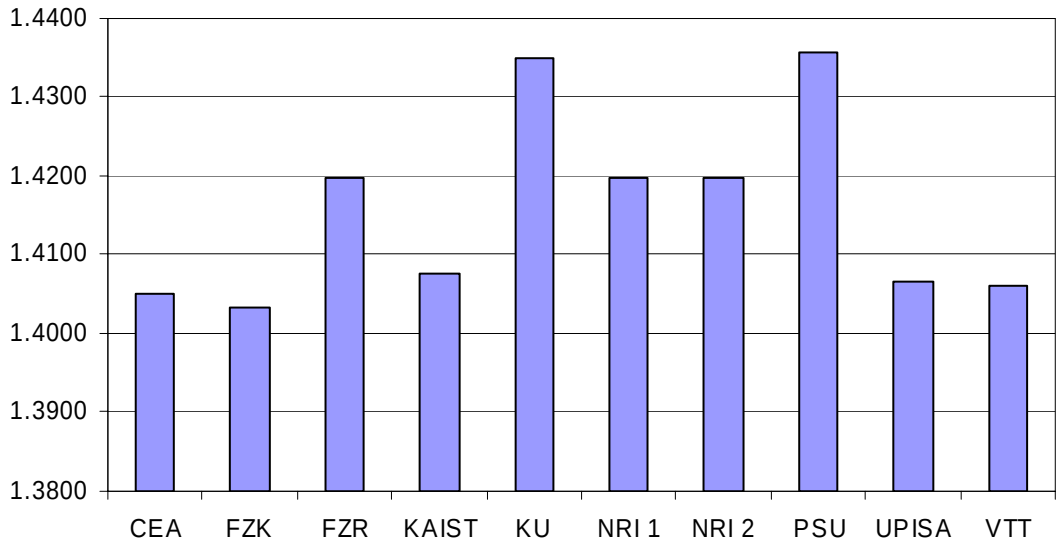

Table 4.3. Participant deviations and figure of merit for HZP RPF

Participant	RPF	Deviation	FOM
CEA	1.405	-0.011	-0.90
FZK	1.403	-0.012	-1.03
FZR	1.420	0.004	0.32
KAIST	1.408	-0.008	-0.68
KU	1.435	0.019	1.57
NRI 1	1.420	0.004	0.32
NRI 2	1.420	0.004	0.32
PSU	1.436	0.020	1.64
UPISA	1.407	-0.009	-0.76
VTT	1.406	-0.010	-0.81
Mean	1.416	–	–
Standard deviation	0.012	–	–

Figure 4.3. HZP axial peaking factor (APF) comparison

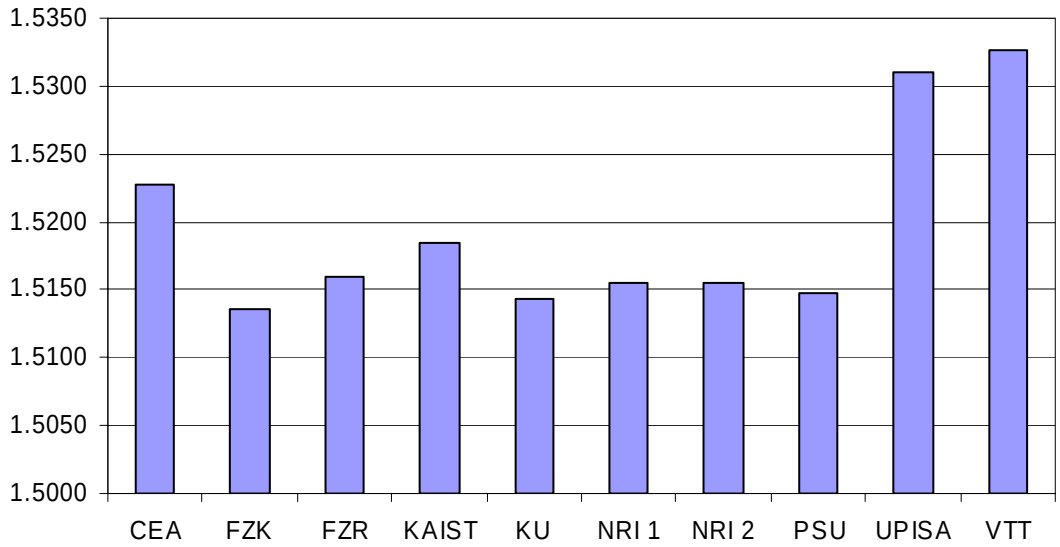

Table 4.4. Participant deviations and figure of merit for HZP APF

Participant	APF	Deviation	FOM
CEA	1.523	0.003	0.47
FZK	1.514	-0.006	-0.83
FZR	1.516	-0.003	-0.49
KAIST	1.519	-0.001	-0.13
KU	1.514	-0.005	-0.73
NRI 1	1.516	-0.004	-0.56
NRI 2	1.516	-0.004	-0.56
PSU	1.515	-0.005	-0.67
UPISA	1.531	0.012	1.64
VTT	1.533	0.013	1.88
Mean	1.519	–	–
Standard deviation	0.007	–	–

Figure 4.4. HZP axial offset (AO) comparison

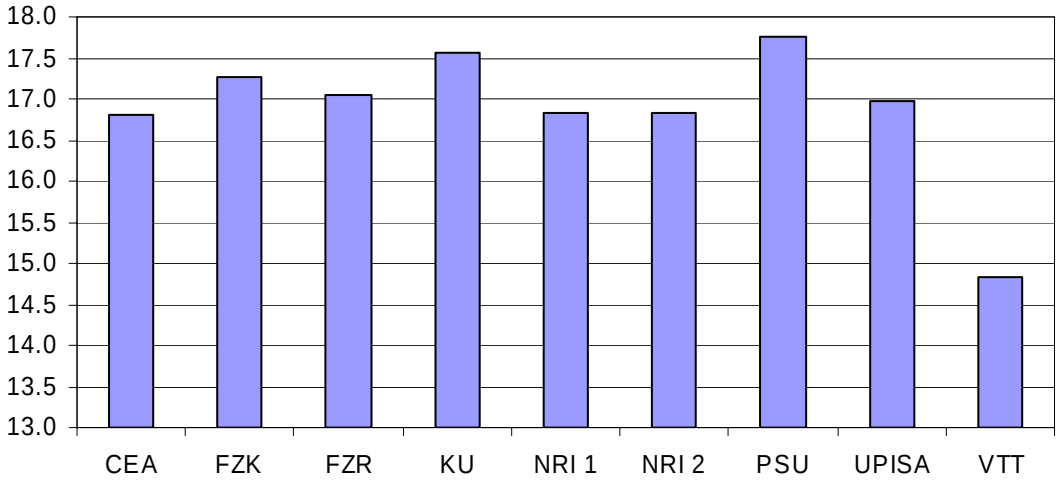

Table 4.5. Participant deviations and figure of merit for HZP AO

Participant	AO	Deviation	FOM
CEA	16.81	-0.08	-0.09
FZK	17.27	0.39	0.46
FZR	17.06	0.18	0.21
KU	17.57	0.69	0.82
NRI 1	16.84	-0.04	-0.05
NRI 2	16.84	-0.04	-0.05
PSU	17.75	0.87	1.04
UPISA	16.97	0.09	0.11
VTT	14.83	-2.05	-2.44
Mean	16.88	–	–
Standard deviation	0.84	–	–

Figure 4.5. HZP ejected rod worth (ERW) comparison

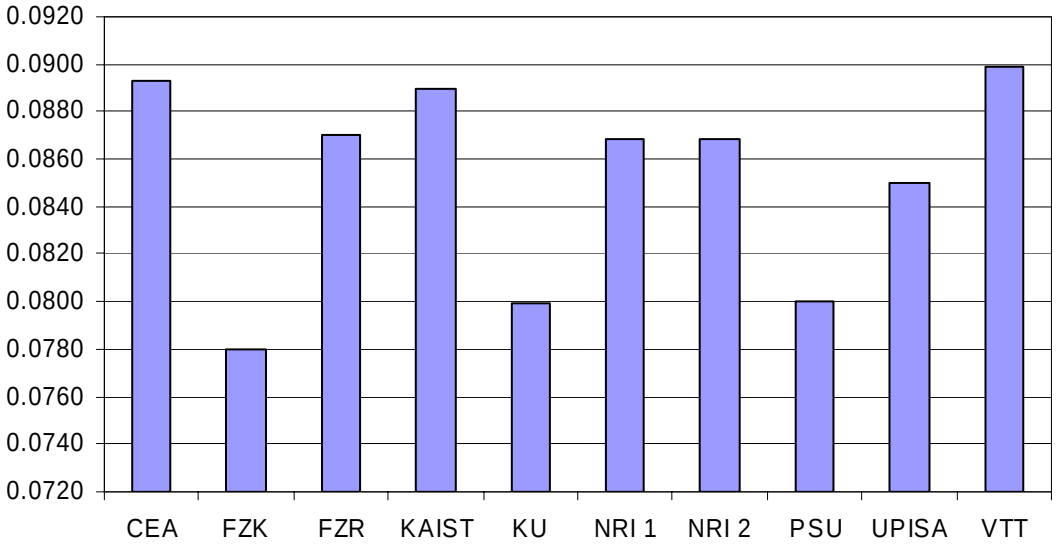

Table 4.6. Participant deviations and figure or merit for HZP ERW

Participant	ERW	Deviation	FOM
CEA	0.0893	0.0041	0.96
FZK	0.0780	-0.0072	-1.66
FZR	0.0870	0.0018	0.42
KAIST	0.0889	0.0038	0.87
KU	0.0799	-0.0052	-1.21
NRI 1	0.0868	0.0016	0.38
NRI 2	0.0868	0.0016	0.38
PSU	0.0800	-0.0052	-1.20
UPISA	0.0850	-0.0002	-0.04
VTT	0.0899	0.0047	1.09
Mean	0.0852	–	–
Standard Deviation	0.0043	–	–

Figure 4.6. HZP control rod group 10 worth (CR 10 W) comparison

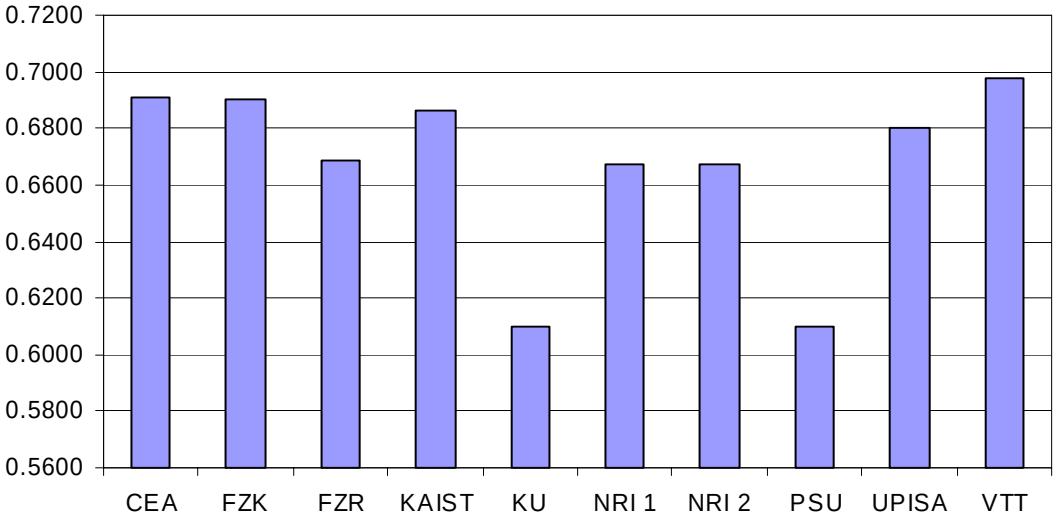

Table 4.7. Participant deviations and figure of merit for HZP CR 10 W

Participant	CR 10 W	Deviation	FOM
CEA	0.6911	0.0242	0.76
FZK	0.6900	0.0230	0.73
FZR	0.6690	0.0020	0.06
KAIST	0.6863	0.0194	0.61
KU	0.6102	-0.0567	-1.79
NRI 1	0.6677	0.0007	0.02
NRI 2	0.6677	0.0007	0.02
PSU	0.6100	-0.0570	-1.79
UPISA	0.6800	0.0130	0.41
VTT	0.6976	0.0306	0.97
Mean	0.6670	–	–
Standard deviation	0.0317	–	–

Figure 4.7. HZP tripped rod worth (TRW) comparison

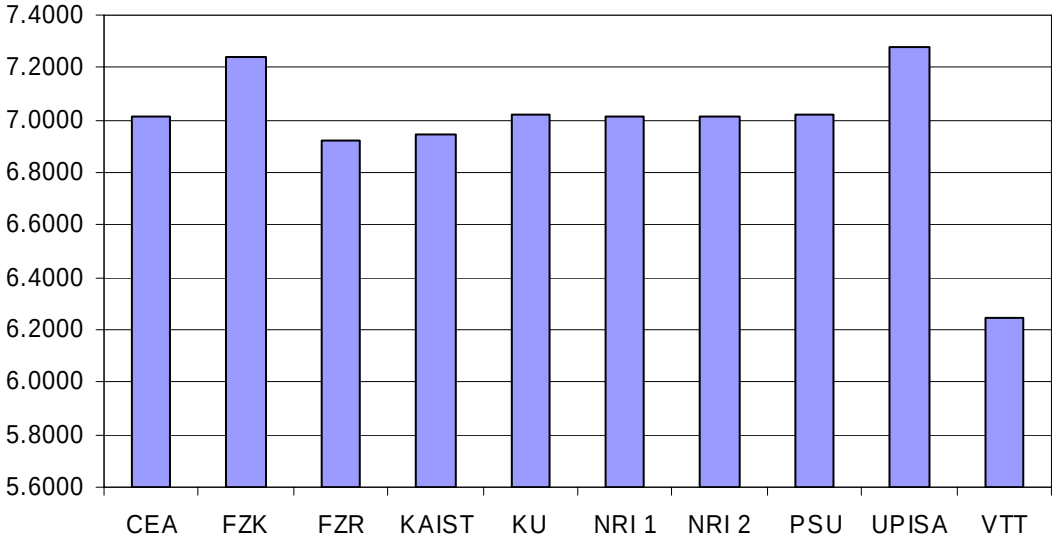

Table 4.8. Participant deviations and figure of merit for HZP TRW

Participant	TRW	Deviation	FOM
CEA	7.0116	0.0405	0.14
FZK	7.2440	0.2729	0.97
FZR	6.9200	-0.0511	-0.18
KAIST	6.9433	-0.0278	-0.10
KU	7.0178	0.0467	0.17
NRI 1	7.0128	0.0417	0.15
NRI 2	7.0128	0.0417	0.15
PSU	7.0200	0.0489	0.17
UPISA	7.2800	0.3089	1.10
VTT	6.2484	-0.7227	-2.58
Mean	6.9711	–	–
Standard deviation	0.2799	–	–

Figure 4.8. HZP axial power distribution (APD) comparisons

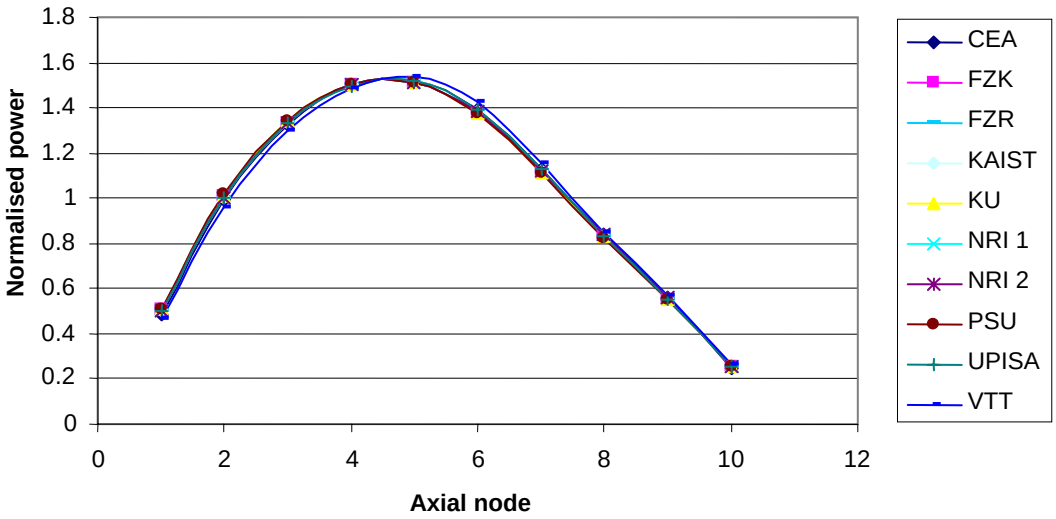

Table 4.9. Participant deviations from mean for HZP APD

	CEA	FZK	FZR	KAIST	KU	NRI 1	NRI 2	PSU	UPISA	VTT	Mean	St dev.
1	-0.014	0.010	0.002	0.002	0.013	0.000	0.000	0.015	0.006	-0.034	0.497	0.0144
2	-0.008	0.009	0.004	0.005	0.013	0.001	0.001	0.016	0.001	-0.042	0.999	0.0161
3	-0.002	0.005	0.003	0.007	0.009	0.000	0.000	0.011	-0.001	-0.031	1.330	0.0117
4	0.003	0.000	0.001	0.005	0.003	-0.001	-0.001	0.005	-0.002	-0.011	1.500	0.0047
5	0.005	-0.004	-0.002	0.000	-0.004	-0.003	-0.003	-0.004	-0.001	0.014	1.518	0.0057
6	0.004	-0.008	-0.005	-0.004	-0.010	-0.004	-0.004	-0.011	0.004	0.038	1.387	0.0142
7	0.006	-0.007	-0.003	-0.005	-0.011	-0.001	-0.001	-0.013	0.003	0.031	1.123	0.0122
8	0.007	-0.003	0.000	-0.003	-0.008	0.003	0.003	-0.010	-0.005	0.017	0.836	0.0079
9	0.002	-0.001	0.000	-0.004	-0.005	0.003	0.003	-0.007	-0.004	0.010	0.555	0.0050
10	-0.004	0.001	-0.001	-0.003	0.000	0.001	0.001	-0.001	-0.001	0.008	0.254	0.0031

Table 4.10. Participant figure of merit for HZP APD

	CEA	FZK	FZR	KAIST	KU	NRI 1	NRI 2	PSU	UPISA	VTT
1	-0.94	0.67	0.12	0.16	0.91	0.02	0.02	1.01	0.39	-2.37
2	-0.50	0.55	0.25	0.34	0.79	0.07	0.07	0.97	0.05	-2.59
3	-0.19	0.41	0.26	0.56	0.75	-0.02	-0.02	0.97	-0.10	-2.62
4	0.63	-0.01	0.22	0.97	0.63	-0.30	-0.30	0.97	-0.33	-2.45
5	0.83	-0.73	-0.31	0.05	-0.68	-0.48	-0.48	-0.61	-0.12	2.52
6	0.28	-0.56	-0.32	-0.30	-0.71	-0.26	-0.26	-0.78	0.25	2.66
7	0.49	-0.57	-0.24	-0.38	-0.87	-0.04	-0.04	-1.06	0.21	2.51
8	0.84	-0.40	-0.02	-0.42	-0.99	0.37	0.37	-1.32	-0.59	2.15
9	0.49	-0.19	0.09	-0.72	-0.91	0.67	0.67	-1.33	-0.79	2.02
10	-1.18	0.35	-0.19	-1.00	-0.13	0.32	0.32	-0.48	-0.44	2.41

Figure 4.9. HP-SS k_{eff} comparison

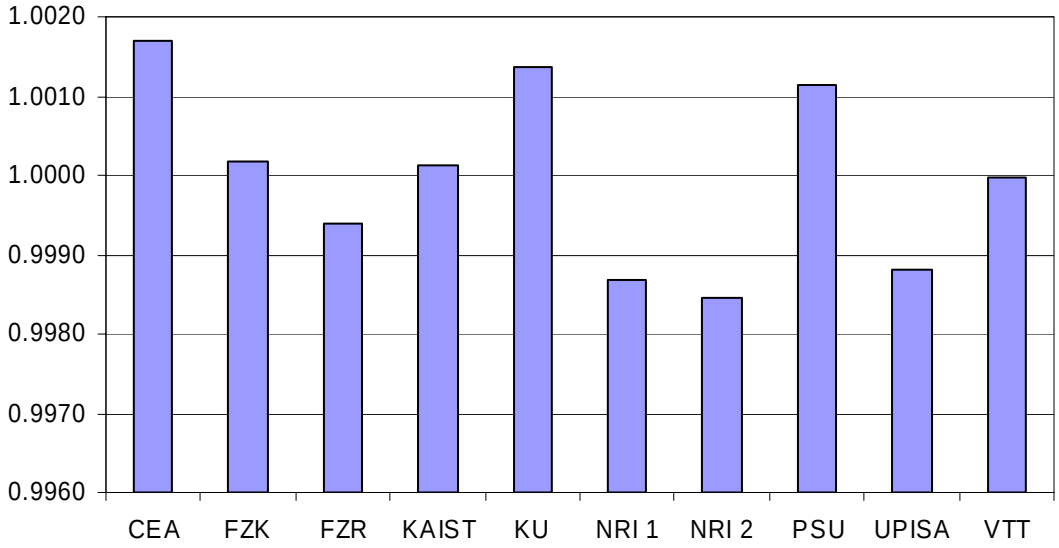

Table 4.11. Participant deviations and figure of merit for HP-SS k_{eff}

Participant	k_{eff}	Deviation	FOM
CEA	1.00170	0.00172	1.48
FZK	1.00019	0.00020	0.18
FZR	0.99938	-0.00060	-0.52
KAIST	1.00013	0.00015	0.13
KU	1.00137	0.00139	1.20
NRI 1	0.99867	-0.00131	-1.13
NRI 2	0.99845	-0.00153	-1.32
PSU	1.00115	0.00117	1.01
UPISA	0.99881	-0.00117	-1.01
VTT	0.99997	-0.00002	-0.01
Mean	0.99998	–	–
Standard deviation	0.00116	–	–

Figure 4.10. HP-SS radial peaking factor (RPF) comparison

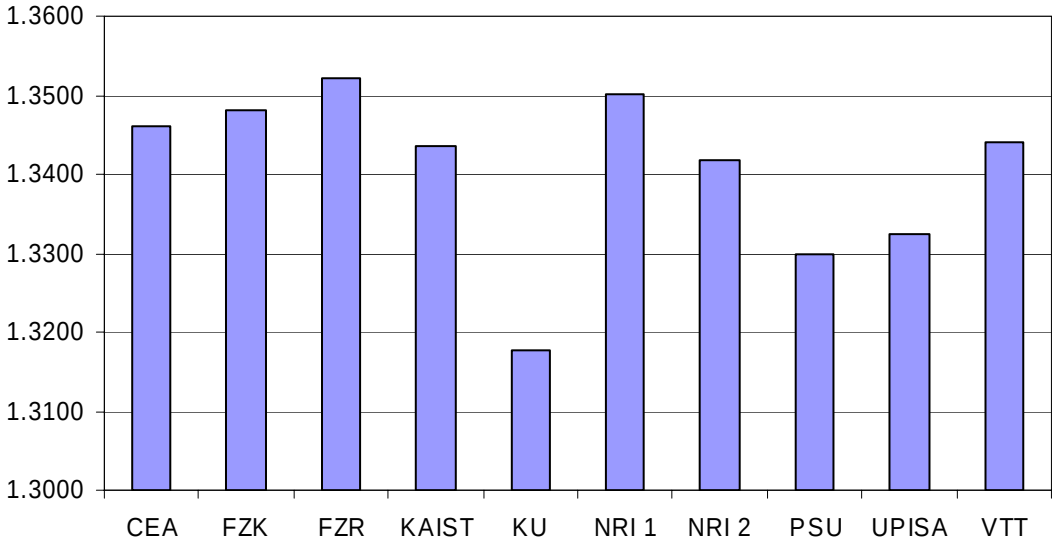

Table 4.12. Participant deviations and figure of merit for HP-SS RPF

Participant	RPF	Deviation	FOM
CEA	1.346	0.005	0.51
FZK	1.348	0.008	0.71
FZR	1.352	0.012	1.07
KAIST	1.344	0.003	0.27
KU	1.318	-0.023	-2.12
NRI 1	1.350	0.010	0.89
NRI 2	1.342	0.001	0.11
PSU	1.330	-0.011	-1.00
UPISA	1.332	-0.008	-0.77
VTT	1.344	0.004	0.33
Mean	1.341	–	–
Standard deviation	0.011	–	–

Figure 4.11. HP-SS axial peaking factor (APF) comparison

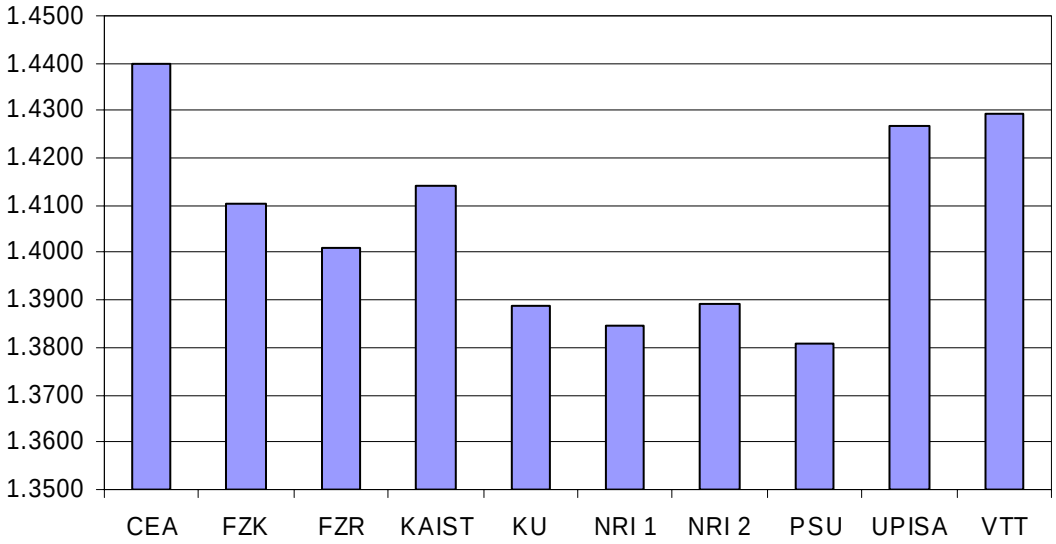

Table 4.13. Participant deviations and figure of merit for HP-SS APF

Participant	APF	Deviation	FOM
CEA	1.440	0.034	1.61
FZK	1.410	0.004	0.18
FZR	1.401	-0.005	-0.26
KAIST	1.414	0.008	0.36
KU	1.389	-0.017	-0.84
NRI 1	1.385	-0.022	-1.05
NRI 2	1.389	-0.017	-0.83
PSU	1.381	-0.026	-1.24
UPISA	1.427	0.020	0.97
VTT	1.429	0.023	1.10
Mean	1.406	–	–
Standard deviation	0.021	–	–

Figure 4.12. HP-SS axial offset (AO) comparison

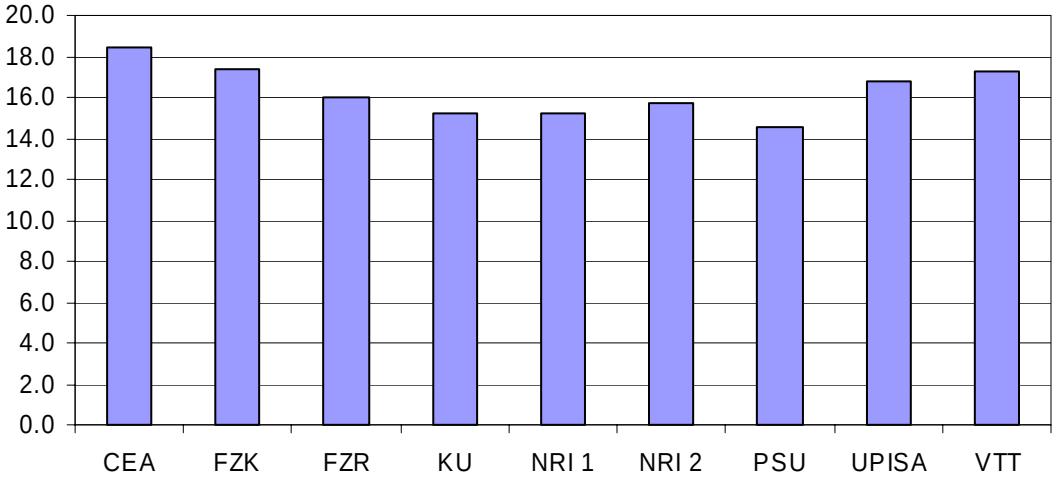

Table 4.14. Participant deviations and figure of merit for HP-SS AO

Participant	AO	Deviation	FOM
CEA	18.48	2.19	1.71
FZK	17.36	1.07	0.84
FZR	16.00	-0.29	-0.22
KU	15.20	-1.09	-0.85
NRI 1	15.21	-1.07	-0.84
NRI 2	15.68	-0.61	-0.47
PSU	14.54	-1.75	-1.37
UPISA	16.82	0.53	0.42
VTT	17.29	1.01	0.79
Mean	16.29	–	–
Standard deviation	1.28	–	–

Figure 4.13. HP-SS axial power distribution (APD) comparisons

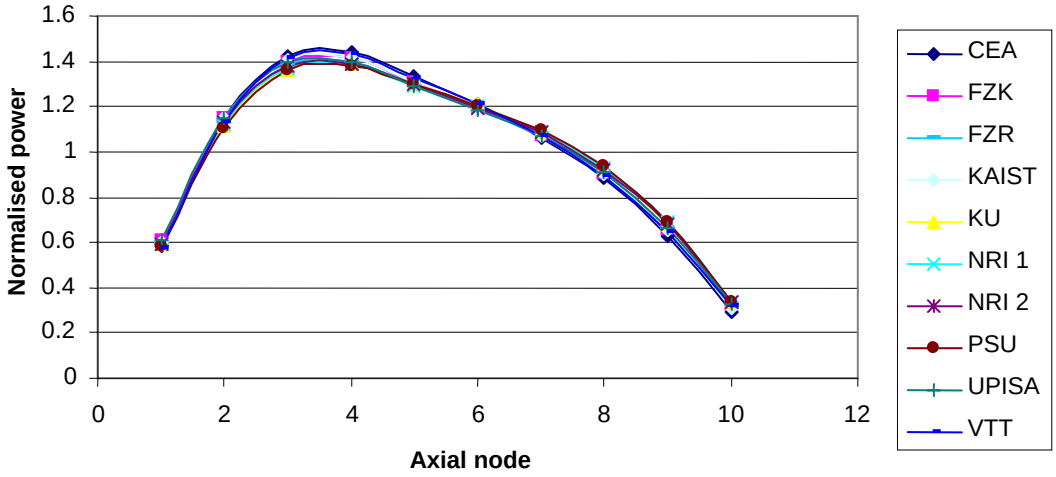

Table 4.15. Participant deviations from mean for HP-SS APD

	CEA	FZK	FZR	KAIST	KU	NRI 1	NRI 2	PSU	UPISA	VTT	Mean	St. dev
1	-0.008	0.014	0.003	0.006	-0.004	-0.002	0.002	-0.009	0.018	-0.020	0.593	0.0112
2	0.014	0.014	0.003	0.013	-0.019	-0.010	-0.003	-0.024	0.014	-0.003	1.132	0.0143
3	0.033	0.010	-0.001	0.015	-0.023	-0.020	-0.013	-0.031	0.008	0.022	1.389	0.0212
4	0.036	0.006	-0.003	0.010	-0.015	-0.019	-0.015	-0.023	-0.005	0.026	1.404	0.0197
5	0.026	0.001	-0.002	0.005	-0.002	-0.011	-0.010	-0.008	-0.015	0.017	1.305	0.0128
6	0.007	-0.006	-0.003	-0.003	0.007	-0.001	-0.004	0.006	-0.014	0.012	1.200	0.0078
7	-0.013	-0.010	-0.001	-0.009	0.013	0.010	0.005	0.019	-0.008	-0.006	1.078	0.0113
8	-0.030	-0.013	0.001	-0.013	0.016	0.019	0.012	0.027	-0.002	-0.018	0.911	0.0186
9	-0.037	-0.011	0.002	-0.014	0.016	0.021	0.016	0.027	0.002	-0.022	0.665	0.0206
10	-0.028	-0.005	0.000	-0.009	0.010	0.012	0.009	0.016	0.004	-0.009	0.323	0.0131

Table 4.16. Participant figure of merit for HP-SS APD

	CEA	FZK	FZR	KAIST	KU	NRI 1	NRI 2	PSU	UPISA	VTT
1	-0.74	1.27	0.28	0.54	-0.34	-0.19	0.18	-0.82	1.58	-1.76
2	0.99	0.99	0.24	0.92	-1.31	-0.69	-0.21	-1.71	0.96	-0.20
3	1.57	0.49	-0.05	0.68	-1.11	-0.93	-0.61	-1.46	0.37	1.05
4	1.85	0.32	-0.13	0.53	-0.75	-0.97	-0.74	-1.17	-0.24	1.31
5	2.00	0.04	-0.19	0.36	-0.13	-0.83	-0.76	-0.60	-1.21	1.32
6	0.84	-0.83	-0.36	-0.44	0.87	-0.14	-0.48	0.79	-1.80	1.55
7	-1.19	-0.92	-0.08	-0.80	1.17	0.91	0.43	1.71	-0.70	-0.53
8	-1.62	-0.69	0.05	-0.70	0.88	1.03	0.67	1.47	-0.12	-0.97
9	-1.79	-0.53	0.10	-0.67	0.76	1.04	0.76	1.30	0.10	-1.05
10	-2.11	-0.38	0.02	-0.72	0.79	0.90	0.69	1.21	0.27	-0.67

Figure 4.14. Radial peaking factor (RPF) comparison at 15 seconds

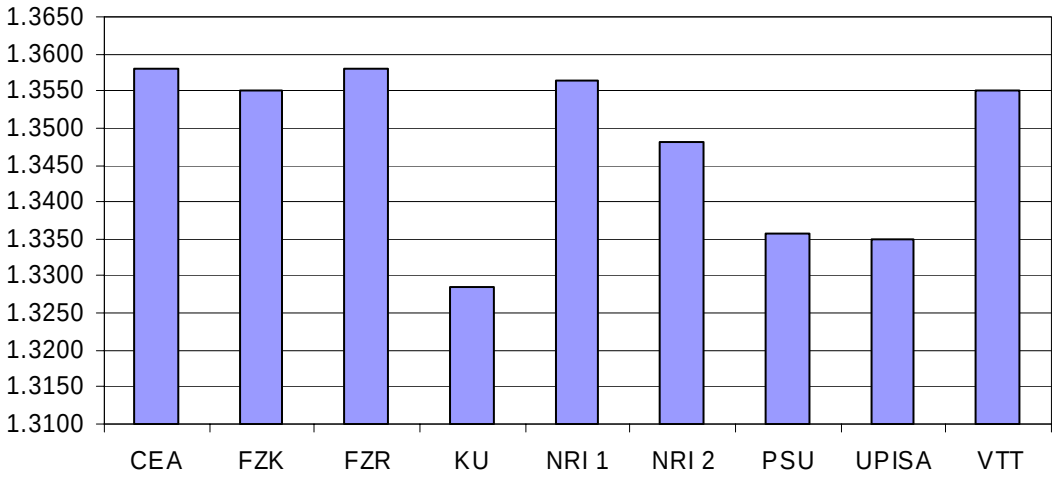

Table 4.17. Participant deviations and figure of merit for RPF at 15 seconds

Participant	RPF	Deviation	FOM
CEA	1.358	0.010	0.88
FZK	1.355	0.007	0.64
FZR	1.358	0.010	0.88
KU	1.329	-0.019	-1.66
NRI 1	1.356	0.008	0.74
NRI 2	1.348	0.000	0.03
PSU	1.336	-0.012	-1.04
UPISA	1.335	-0.013	-1.11
VTT	1.355	0.007	0.64
Mean	1.348	–	–
Standard deviation	0.012	–	–

Figure 4.15. Axial peaking factor (APF) comparison at 15 seconds

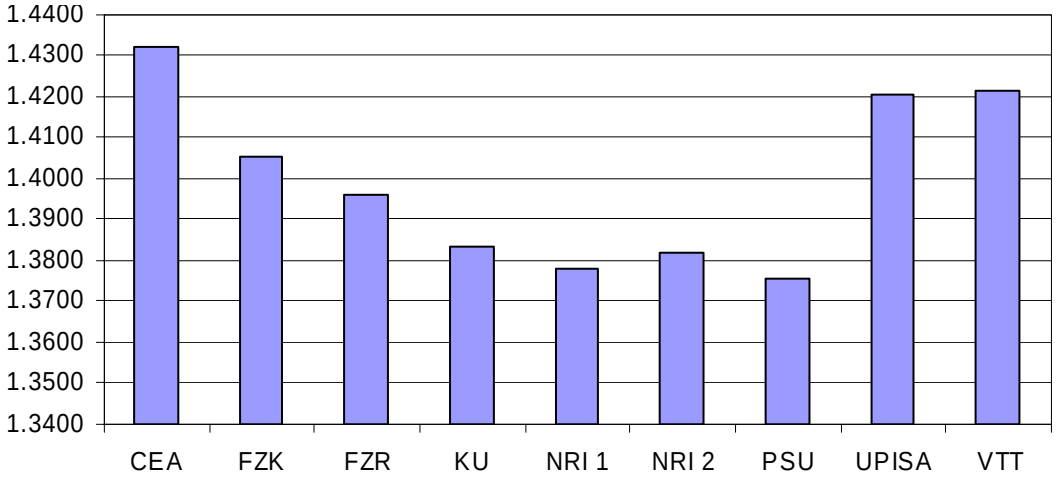

Table 4.18. Participant deviations and figure of merit for APF at 15 seconds

Participant	APF	Deviation	FOM
CEA	1.432	0.033	1.53
FZK	1.406	0.006	0.29
FZR	1.396	-0.004	-0.17
KU	1.384	-0.016	-0.74
NRI 1	1.378	-0.021	-1.00
NRI 2	1.382	-0.018	-0.82
PSU	1.376	-0.024	-1.12
UPISA	1.420	0.021	0.98
VTT	1.422	0.022	1.05
Mean	1.399	–	–
Standard deviation	0.021	–	–

Figure 4.16. Axial offset (AO) comparison at 15 seconds

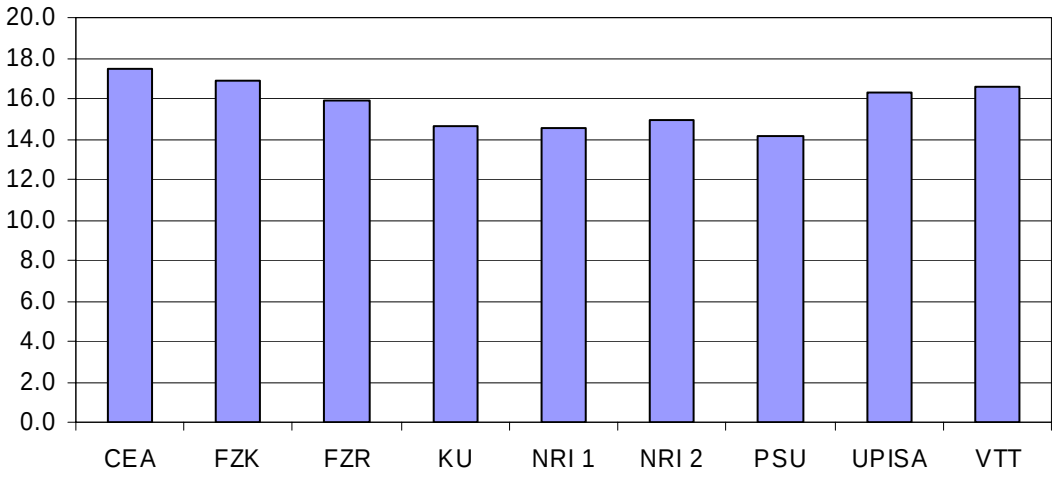

Table 4.19. Participant deviations and figure of merit for AO at 15 seconds

Participant	AO	Deviation	FOM
CEA	17.49	1.78	1.51
FZK	16.86	1.15	0.97
FZR	15.92	0.21	0.18
KU	14.61	-1.10	-0.93
NRI 1	14.55	-1.16	-0.98
NRI 2	14.96	-0.75	-0.63
PSU	14.14	-1.57	-1.33
UPISA	16.32	0.61	0.52
VTT	16.54	0.83	0.70
Mean	15.71	–	–
Standard deviation	1.18	–	–

Figure 4.17. Axial power distribution (APD) comparisons at 15 seconds

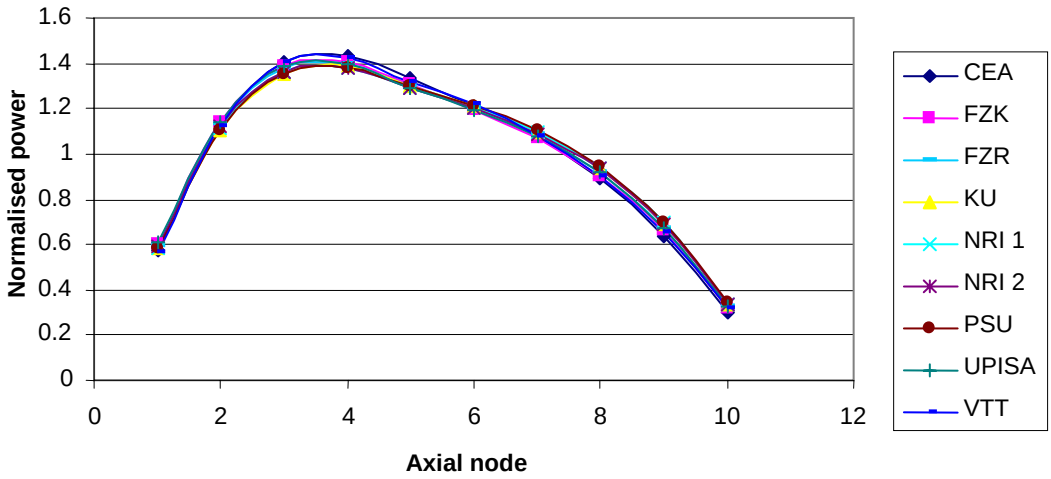

Table 4.20. Participant deviations from mean for APD at 15 seconds

	CEA	FZK	FZR	KU	NRI 1	NRI 2	PSU	UPISA	VTT	Mean	St dev
1	-0.012	0.016	0.005	-0.003	-0.001	0.002	-0.007	0.020	-0.019	0.586	0.0123
2	0.009	0.017	0.006	-0.017	-0.009	-0.002	-0.020	0.017	-0.001	1.121	0.0136
3	0.029	0.014	0.002	-0.021	-0.019	-0.013	-0.027	0.011	0.024	1.378	0.0207
4	0.035	0.009	-0.001	-0.013	-0.019	-0.015	-0.021	-0.002	0.027	1.397	0.0201
5	0.028	0.002	-0.002	-0.001	-0.011	-0.010	-0.008	-0.015	0.018	1.303	0.0141
6	0.009	-0.007	-0.004	0.006	-0.002	-0.004	0.004	-0.015	0.012	1.204	0.0085
7	-0.009	-0.013	-0.003	0.012	0.010	0.005	0.015	-0.011	-0.007	1.086	0.0107
8	-0.026	-0.016	-0.001	0.015	0.019	0.013	0.022	-0.005	-0.020	0.921	0.0179
9	-0.035	-0.015	0.000	0.014	0.021	0.016	0.022	-0.001	-0.024	0.675	0.0205
10	-0.027	-0.006	-0.001	0.009	0.012	0.009	0.013	0.002	-0.010	0.328	0.0131

Table 4.21. Participant figure of merit for APD at 15 seconds

	CEA	FZK	FZR	KU	NRI 1	NRI 2	PSU	UPIA	VTT
1	-1.00	1.26	0.39	-0.25	-0.12	0.20	-0.55	1.59	-1.52
2	0.66	1.25	0.47	-1.24	-0.64	-0.18	-1.50	1.25	-0.07
3	1.39	0.67	0.09	-1.03	-0.90	-0.61	-1.31	0.53	1.16
4	1.75	0.46	-0.05	-0.66	-0.93	-0.74	-1.05	-0.12	1.34
5	1.95	0.11	-0.15	-0.06	-0.76	-0.73	-0.55	-1.06	1.26
6	1.09	-0.79	-0.44	0.75	-0.21	-0.51	0.43	-1.72	1.41
7	-0.83	-1.20	-0.25	1.14	0.91	0.45	1.43	-1.01	-0.64
8	-1.46	-0.88	-0.08	0.82	1.03	0.71	1.25	-0.29	-1.10
9	-1.68	-0.71	-0.01	0.68	1.03	0.80	1.08	-0.03	-1.15
10	-2.09	-0.48	-0.09	0.69	0.88	0.70	1.00	0.16	-0.78

Figure 4.18. Radial peaking factor (RPF) comparison at 800 seconds

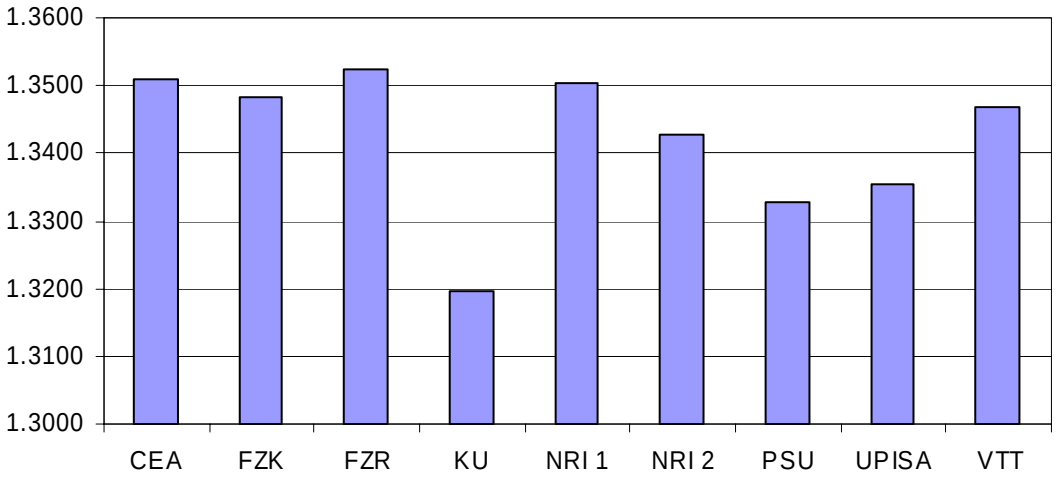

Table 4.22. Participant deviations and figure of merit for RPF at 800 seconds

Participant	RPF	Deviation	FOM
CEA	1.351	0.009	0.81
FZK	1.348	0.006	0.57
FZR	1.352	0.010	0.93
KU	1.320	-0.023	-2.08
NRI 1	1.350	0.008	0.74
NRI 2	1.343	0.001	0.06
PSU	1.333	-0.009	-0.85
UPISA	1.335	-0.007	-0.62
VTT	1.347	0.005	0.42
Mean	1.342	–	–
Standard deviation	0.011	–	–

Figure 4.19. Axial peaking factor (APF) comparison at 800 seconds

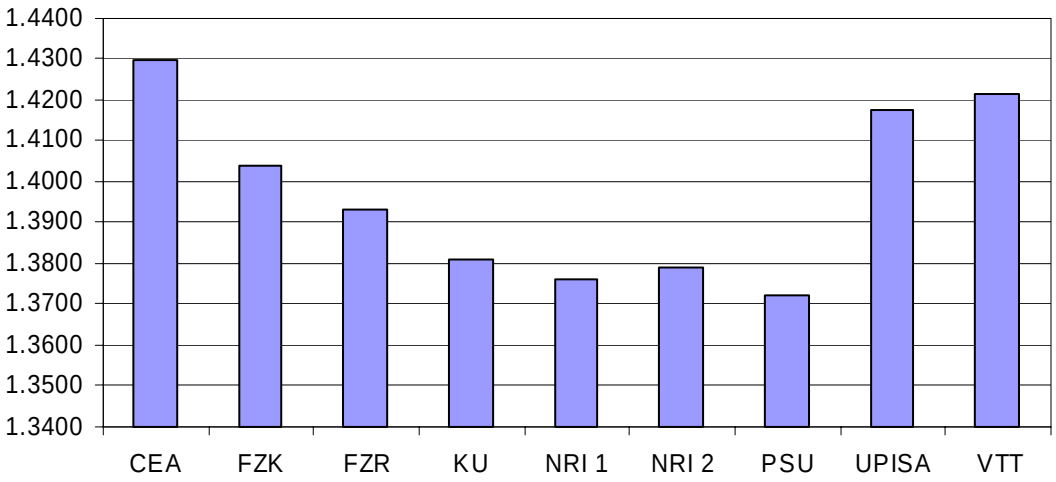

Table 4.23. Participant deviations and figure of merit for APF at 800 seconds

Participant	APF	Deviation	FOM
CEA	1.430	0.033	1.50
FZK	1.404	0.007	0.31
FZR	1.393	-0.004	-0.18
KU	1.381	-0.016	-0.75
NRI 1	1.376	-0.021	-0.97
NRI 2	1.379	-0.018	-0.83
PSU	1.372	-0.025	-1.14
UPISA	1.418	0.020	0.94
VTT	1.422	0.024	1.12
Mean	1.397	–	–
Standard deviation	0.022	–	–

Figure 4.20. Axial offset (AO) comparison at 800 seconds

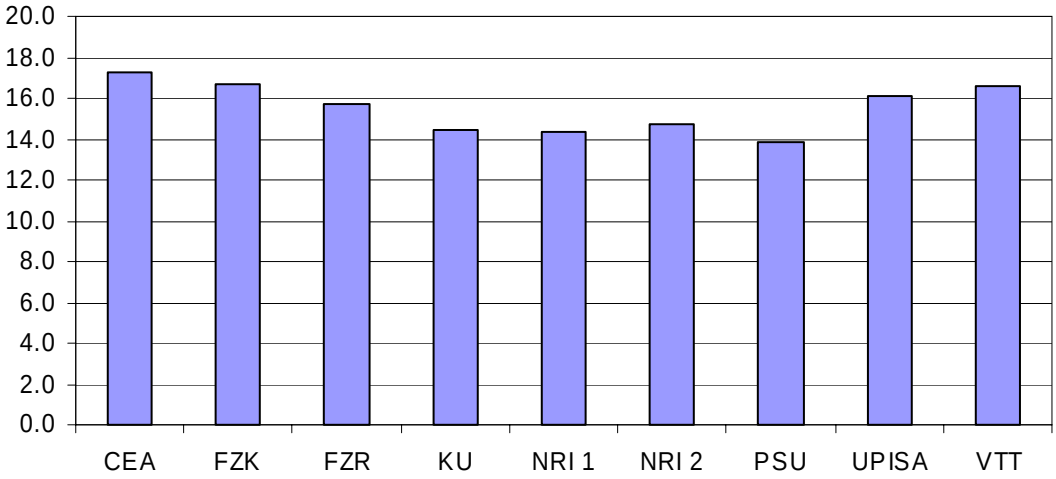

Table 4.24. Participant deviations and figure of merit for AO at 800 seconds

Participant	AO	Deviation	FOM
CEA	17.29	1.77	1.45
FZK	16.72	1.20	0.98
FZR	15.69	0.17	0.14
KU	14.40	-1.12	-0.92
NRI 1	14.37	-1.15	-0.94
NRI 2	14.71	-0.81	-0.66
PSU	13.87	-1.65	-1.35
UPISA	16.11	0.59	0.48
VTT	16.54	1.02	0.83
Mean	15.52	–	–
Standard deviation	1.22	–	–

Figure 4.21. Axial power distribution (APD) comparisons at 800 seconds

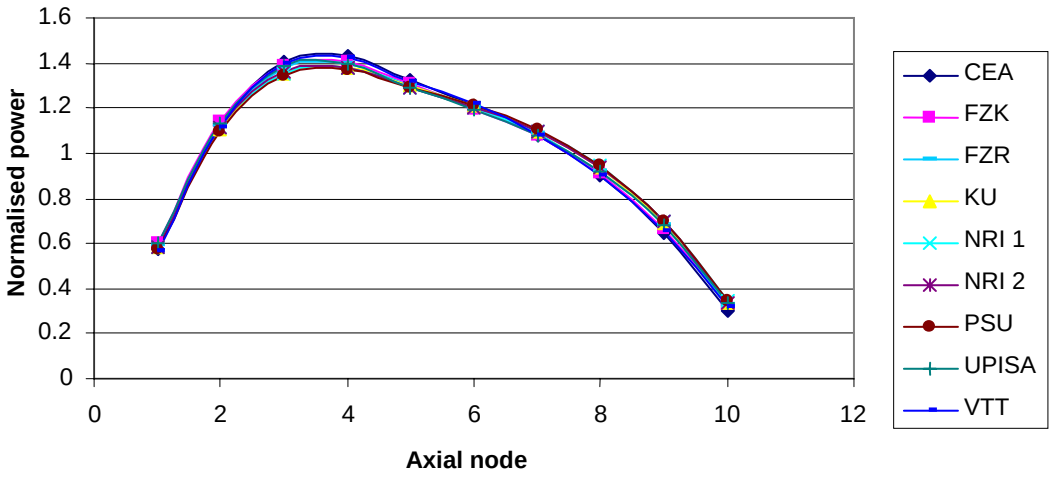

Table 4.25. Participant deviations from mean for APD at 800 seconds

	CEA	FZK	FZR	KU	NRI 1	NRI 2	PSU	UPISA	VTT	Mean	St. dev
1	-0.012	0.016	0.005	-0.003	-0.001	0.002	-0.007	0.019	-0.018	0.585	0.0122
2	0.009	0.019	0.006	-0.017	-0.008	-0.003	-0.021	0.017	0.000	1.118	0.0138
3	0.029	0.015	0.002	-0.021	-0.018	-0.013	-0.028	0.011	0.025	1.375	0.0211
4	0.036	0.010	-0.001	-0.013	-0.018	-0.015	-0.022	-0.002	0.027	1.394	0.0204
5	0.028	0.002	-0.002	-0.001	-0.011	-0.011	-0.008	-0.014	0.018	1.302	0.0141
6	0.010	-0.007	-0.004	0.006	-0.002	-0.004	0.004	-0.015	0.012	1.204	0.0086
7	-0.009	-0.013	-0.003	0.012	0.009	0.005	0.016	-0.010	-0.007	1.088	0.0107
8	-0.026	-0.017	-0.001	0.015	0.018	0.013	0.023	-0.005	-0.020	0.924	0.0183
9	-0.035	-0.016	0.000	0.014	0.021	0.017	0.023	-0.001	-0.024	0.678	0.0210
10	-0.028	-0.007	-0.001	0.009	0.011	0.010	0.014	0.002	-0.010	0.330	0.0134

Table 4.26. Participant figure of merit for APD at 800 seconds

	CEA	FZK	FZR	KU	NRI 1	NRI 2	PSU	UPISA	VTT
1	-1.01	1.30	0.38	-0.24	-0.11	0.17	-0.58	1.58	-1.49
2	0.61	1.34	0.44	-1.21	-0.61	-0.21	-1.53	1.19	-0.02
3	1.37	0.71	0.08	-1.01	-0.87	-0.63	-1.34	0.52	1.17
4	1.74	0.47	-0.06	-0.66	-0.90	-0.75	-1.08	-0.10	1.33
5	1.96	0.11	-0.15	-0.09	-0.75	-0.75	-0.59	-1.02	1.27
6	1.15	-0.83	-0.42	0.72	-0.21	-0.50	0.41	-1.71	1.39
7	-0.83	-1.21	-0.24	1.13	0.87	0.47	1.46	-0.97	-0.68
8	-1.44	-0.91	-0.06	0.81	1.00	0.73	1.27	-0.29	-1.10
9	-1.66	-0.74	0.00	0.67	1.00	0.81	1.11	-0.03	-1.16
10	-2.07	-0.53	-0.07	0.70	0.85	0.72	1.03	0.15	-0.78

Figure 4.22. Time history of power

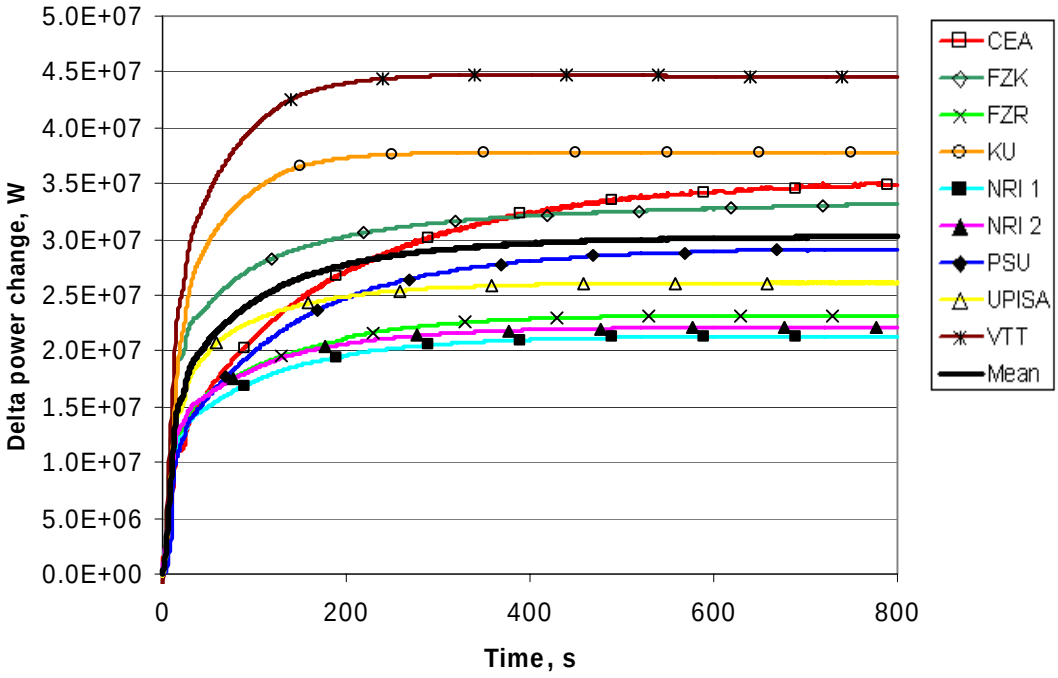

Table 4.27. Power initial value and FOM

	Participant	Initial value, W	ME	VE	MSE	Combined
1	CEA	8.240E+08	0.949410	0.990632	0.987865	0.975968
2	FZK	8.240E+08	0.918107	0.999849	0.991958	0.969970
3	FZR	8.240E+08	0.824134	0.998737	0.955292	0.926053
4	KU	8.240E+08	0.787050	0.997573	0.929681	0.904767
5	NRI-1	8.240E+08	0.788695	0.997704	0.931031	0.905809
6	NRI-2	8.240E+08	0.807814	0.997616	0.944298	0.916575
7	PSU	8.240E+08	0.932937	0.998299	0.993178	0.974804
8	UPISA	8.240E+08	0.902980	0.998790	0.987406	0.963058
9	VTT	8.240E+08	0.673175	0.995801	0.806503	0.825159

Figure 4.23. Time history of fission power

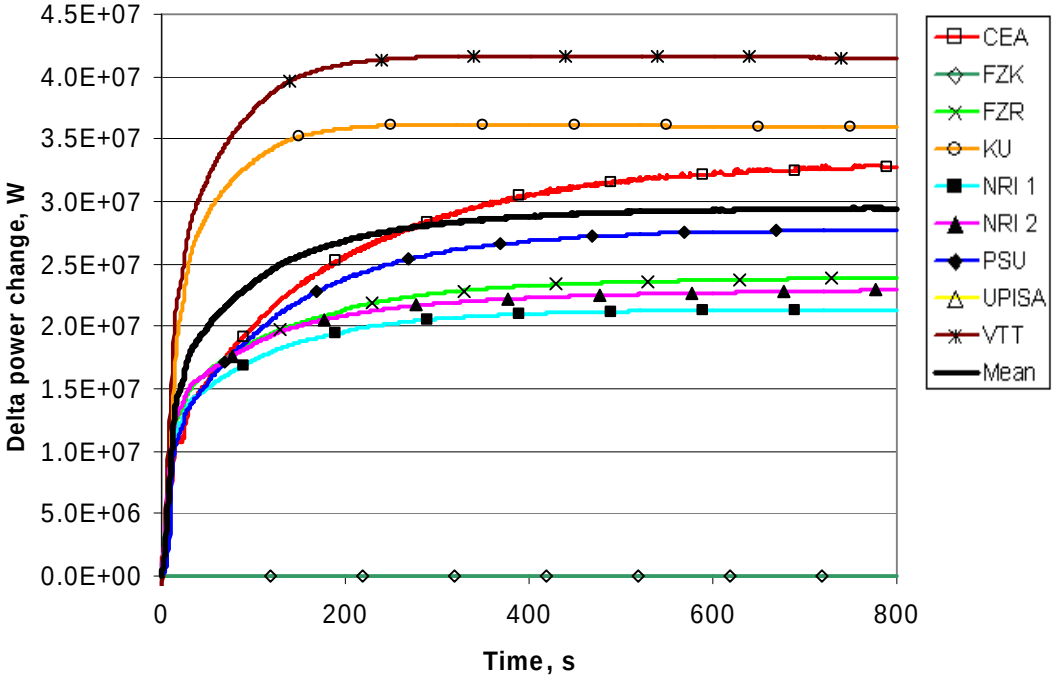

Table 4.28. Fission power initial value and FOM

	Participant	Initial value, W	ME	VE	MSE	Combined
1	CEA	7.654E+08	0.975439	0.992795	0.992179	0.986803
2	FZR	7.653E+08	0.849405	0.998953	0.968542	0.938966
3	KU	7.673E+08	0.796950	0.997391	0.936744	0.910361
4	NRI-1	7.637E+08	0.801978	0.997661	0.940459	0.913365
5	NRI-2	7.653E+08	0.832280	0.997956	0.959089	0.929774
6	PSU	7.651E+08	0.923652	0.999031	0.992259	0.971646
7	VTT	7.680E+08	0.700072	0.996718	0.842576	0.846454

Figure 4.24. Time history of core average fuel temperature

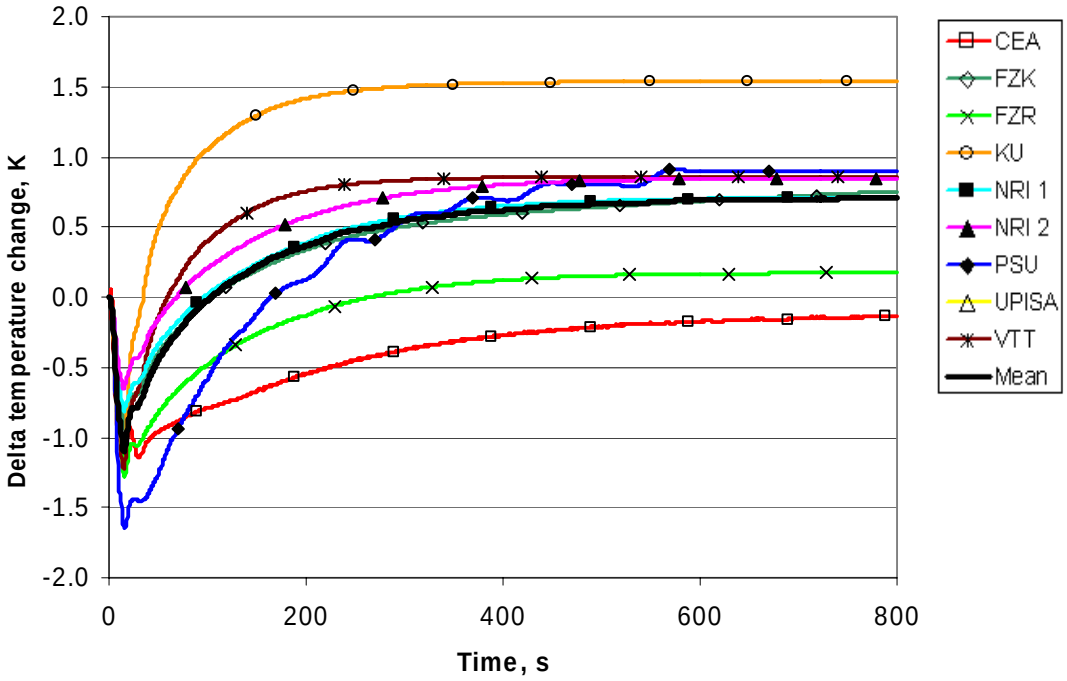

Table 4.29. Core average fuel temperature initial value and FOM

	Participant	Initial value, K	ME	VE	MSE	Combined
1	CEA	597.09	0.687733	0.990093	0.822262	0.833362
2	FZK	658.42	0.997687	0.999611	0.999607	0.998967
3	FZR	678.75	0.789086	0.998050	0.931623	0.906252
4	KU	660.14	0.670347	0.990172	0.798885	0.819800
5	NRI-1	712.07	0.983126	0.999511	0.999217	0.993951
6	NRI-2	711.92	0.906513	0.999229	0.988723	0.964821
7	PSU	677.00	0.978515	0.974143	0.973717	0.975457
8	VTT	641.82	0.882175	0.996214	0.978824	0.952403

Figure 4.25. Time history of core average moderator density

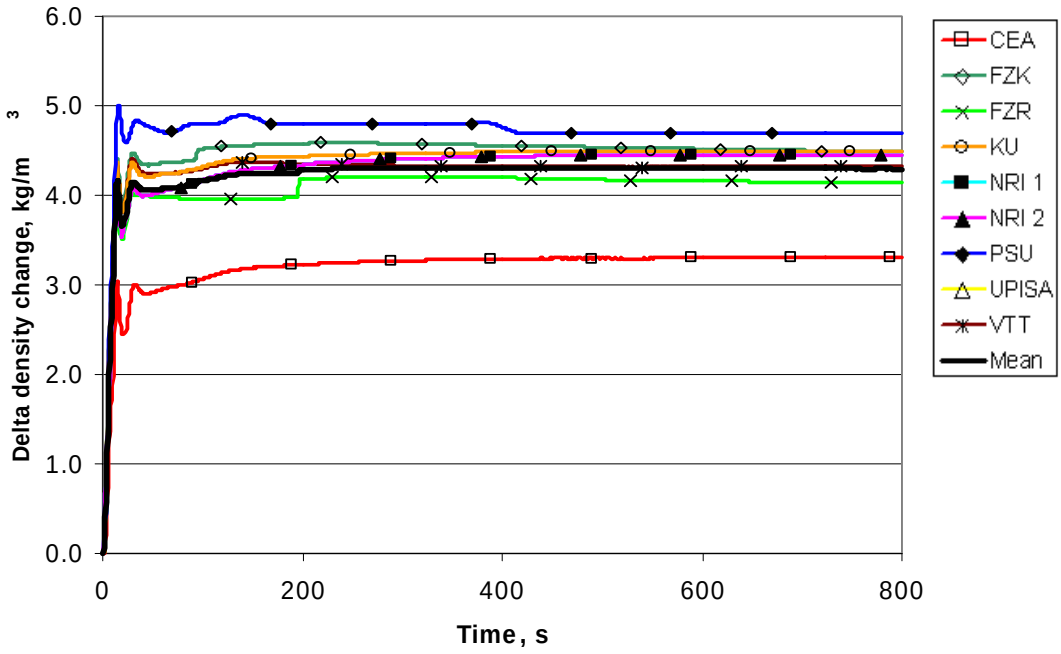

Table 4.30. Core average moderator density initial value and FOM

	Participant	Initial value, kg/m^3	ME	VE	MSE	Combined
1	CEA	754.80	0.807860	0.999634	0.946134	0.917875
2	FZK	748.91	0.944746	0.999883	0.996475	0.980367
3	FZR	751.12	0.968592	0.999844	0.998794	0.989076
4	KU	749.23	0.960343	0.999966	0.998264	0.986190
5	NRI-1	750.28	0.977061	0.999766	0.999215	0.992013
6	NRI-2	750.28	0.977061	0.999766	0.999215	0.992013
7	PSU	748.80	0.900013	0.999296	0.987123	0.962143
8	VTT	750.05	0.987718	0.999824	0.999670	0.995736

Figure 4.26. Time history of maximum nodal average fuel temperature

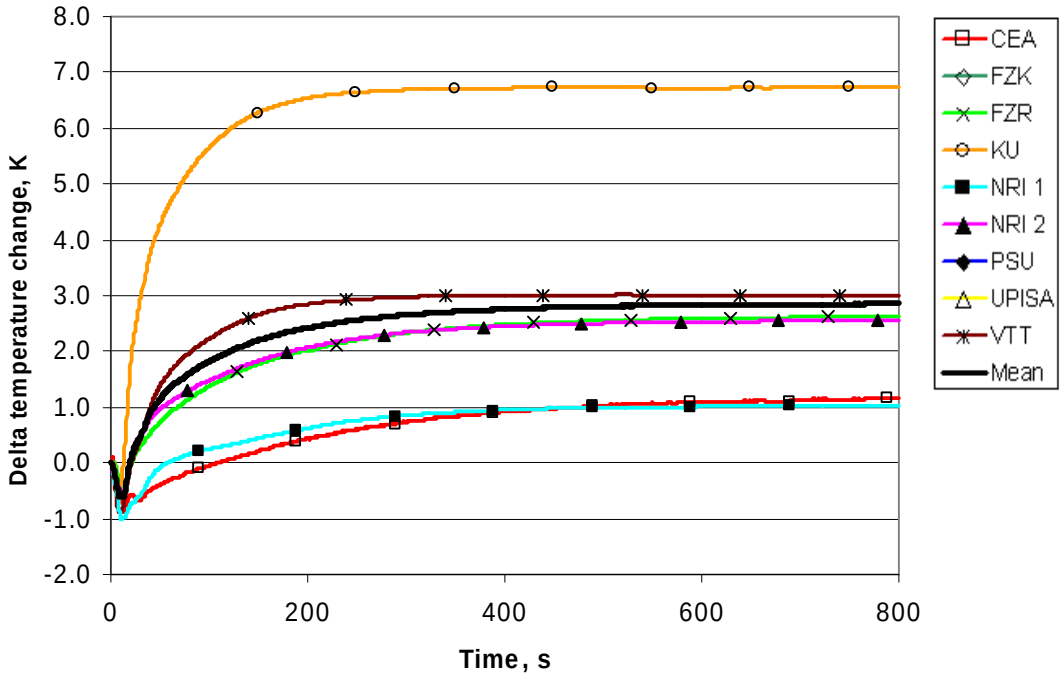

Table 4.31. Maximum nodal average fuel temperature initial value and FOM

	Participant	Initial value, K	ME	VE	MSE	Combined
1	CEA	631.86	0.663970	0.991637	0.790794	0.815466
2	FZR	773.35	0.922671	0.999101	0.992139	0.971303
3	KU	793.29	0.477201	0.968393	0.447861	0.631151
4	NRI-1	778.89	0.669408	0.993393	0.799656	0.820818
5	NRI-2	830.08	0.922127	0.999501	0.992428	0.971351
6	VTT	708.70	0.932267	0.998606	0.993371	0.974747

Chapter 5

ANALYSIS OF OBSERVED DISCREPANCIES IN EXERCISE 2

5.1 Introduction

During the second OECD/DOE/CEA V1000CT benchmark workshop conducted in Sofia, Bulgaria in April 2004 [6], it was discovered that two clusters of participants' results for normalised radial power distribution were formed for both HP-SS conditions and HZP conditions. The observed difference between these two clusters is approximately in the range of ±11%, while the difference within each of the clusters is in the range of ±1.5%. As mentioned in the previous chapter, KU and PSU form one of the clusters of the participants' results, while the rest of the benchmark participants' results form the other cluster. Compared to the results of PWR MSLB benchmark [2], these deviations are not acceptable. Therefore, steps to understand this problem have been taken. These are described in detail in [7]. This chapter of the report shows the results and the observations of this study as well as its most important conclusions.

Two representatives from each cluster were chosen to illustrate the deviations between the participants' results for HZP. To investigate the problem, it was decided to focus only on the HZP state, as it uses fixed thermal-hydraulic feedback. By using HZP, therefore, possible deviations from the thermal-hydraulic modelling are eliminated. The comparison of the PSU (TRAC-PF1/NEM) and CEA (CRONOS2/FLICA4) HZP results for normalised radial power distribution have shown deviations that vary from 11.40% in the periphery of the core to -11.76% in the centre of the core. It was decided that possible sources of the observed deviation could be as follows:

- Differences of the interpolation procedures used for extracting the cross-section values from the cross-section library based on two-dimensional tables as a function of moderator density and fuel temperature.
- The fixed T-H feedback could also be a possible source of deviations if it is not set up properly.
- Position of the control rod groups.
- The equivalence procedure used for fuel assembly homogenisation.
- Differences in the methods for hexagonal geometry used in 3-D neutronics codes.

The first three possible sources of discrepancies, which are all related to the benchmark data interpretation, were eliminated by codes post-checking (cross-section editing). Benchmark data were updated to ensure uniform data interpretation.

Since the VVER-1000 core geometry is too complicated for a direct interpretation of the results, it was decided to define simple benchmark problems in order to analyse the last two possible sources of discrepancies (equivalence procedure and differences in numerical methods).

5.2 Definition of simple benchmark problems

In order to perform sensitivity studies simple test problems were defined. The simple test problems mainly use selected cross-section sets from the V1000CT benchmark library (built with the HELIOS code). These cross-sections are given in Table 5.1. However certain tests (4 and 5) use cross-sections obtained with CASMO-3, which are extracted from the PWR MSLB benchmark cross-section library under the following conditions: T_f = 500.00 K, ρ_{mod} = 769.4675 kg/m^3 (see Table 5.2.). Please note that the cross-sections are divided with ADFs. The reflector cross-section obtained with CASMO-3 for VVER-1000 type reflector is given in the last column. It has material properties that are different from the PWR-type reflector, since it contains more steel.

Table 5.1. Cross-section data with HELIOS

	Cross-sections with ADFs			Cross-sections without ADFs		
	Unrodded	**Rodded**	**Reflector**	**Unrodded**	**Rodded**	**Reflector**
D_1	1.34867E+00	1.30655E+00	0.91038E+00	1.34214E+00	1.36381E+00	0.88356E+00
$\sum_{a1}$	9.15780E-03	1.14440E-02	3.26900E-03	9.11340E-03	1.21199E-02	3.17300E-03
$\upsilon*\sum_{f1}$	5.96278E-03	5.60698E-03	0.00000E+00	5.93391E-03	5.83469E-03	0.00000E+00
$\sum_{s1->2}$	1.71208E-02	1.49700E-02	1.18390E-02	1.70379E-02	1.55193E-02	1.14900E-02
D_2	3.41680E-01	0.27022E+00	0.75490E+00	3.81020E-01	0.38451E+00	0.28256 E+0
$\sum_{a2}$	8.60773E-02	7.76723-02	0.13329E+00	9.59865E-02	1.10473E-01	4.99020E-02
$\upsilon*\sum_{f2}$	1.13965E-01	9.04599E-02	0.00000E+00	1.27084E-01	1.28772E-01	0.00000E+00

Table 5.2. Cross-section data with CASMO-3 (with ADFs)

	Unrodded	**Rodded**	**Reflector**	**VVER reflector**
D_1	.1403427E+01	.1367643E+01	.1005645E+01	.9334416E+00
$\sum_{a1}$	.1176591E-01	.1391181E-01	.1457717E-02	.2816760E-02
$\upsilon*\sum_{f1}$	.5622854E-02	.5377194E-02	.0000000E+00	.0000000E+00
$\sum_{s1->2}$	.1607951E-01	.1351079E-01	.2554830E-01	.1088045E-01
D_2	.3288613E+00	.2510772E+00	.9992122E+00	.9579292E+00
$\sum_{a2}$	.1071855E+00	.9962144E-01	.7161031E-01	.8871995E-01
$\upsilon*\sum_{f2}$	.1458654E+00	.1154028E+00	.0000000E+00	.0000000E+00

Two simple Cartesian and hexagonal geometries are defined:

- *Geometry 1*: 3 × 3 assemblies in Cartesian geometry composed of a centred rodded assembly surrounded by unrodded ones.

- *Geometry 2*: 5 × 5 assemblies in Cartesian geometry composed of a centred rodded assembly surrounded by unrodded ones, surrounded in turn by reflector ones.

- *Geometry 3*: 19 assemblies in hexagonal geometry composed of a entered rodded assembly surrounded by unrodded ones, surrounded in turn by reflector assemblies.

These 3 geometries are described in Figures 5.1-5.3. In Cartesian geometry the assembly pitch is 21.6 cm and in hexagonal geometry it is 23.6 cm across flats.

Figure 5.1. Core plan of the 3 × 3 2-D Cartesian test (geometry 1)

Unrodded	Unrodded	Unrodded
Unrodded	Rodded	Unrodded
Unrodded	Unrodded	Unrodded

Figure 5.2. Core plan of the 5 × 5 2-D Cartesian test (geometry 2)

Reflector	Reflector	Reflector	Reflector	Reflector
Reflector	Unrodded	Unrodded	Unrodded	Reflector
Reflector	Unrodded	Rodded	Unrodded	Reflector
Reflector	Unrodded	Unrodded	Unrodded	Reflector
Reflector	Reflector	Reflector	Reflector	Reflector

Figure 5.3. Core plan of the 2-D hexagonal test (geometry 3)

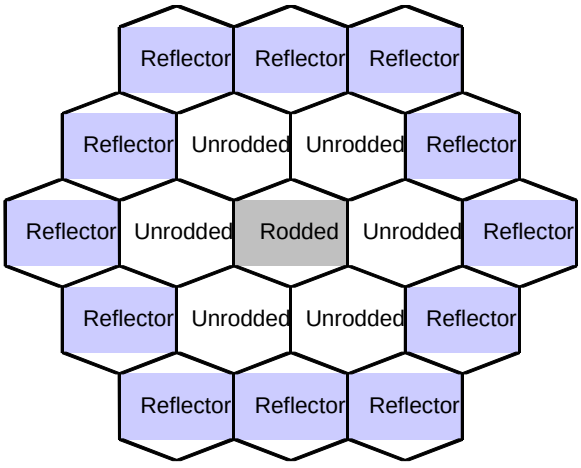

Eight different tests associating different geometries with different sets of cross-sections (with or without ADFs) are defined. Their characteristics are given in Table 5.3.

Table 5.3. Test definitions

Test number	Geometry	Boundary condition	Cross-sections
Test 1-a	1	Reflective	HELIOS with ADFs
Test 1-b	1	Reflective	HELIOS without ADFs
Test 2-a	2	Zero flux	HELIOS with ADFs
Test 2-b	2	Zero flux	HELIOS without ADFs
Test 3-a	3	Zero flux	HELIOS with ADFs
Test 3-b	3	Zero flux	HELIOS without ADFs
Test 4	3	Zero flux	CASMO-3 PWR cross-sections with ADFs
Test 5	3	Zero flux	Fuel: CASMO-3 PWR cross-sections Reflectors: CASMO-3 VVER cross-sections

5.3 Test problem results

The first test (Figures 5.4. and 5.5.) was defined to serve as a standard of comparison. The results show that, provided good spatial convergence, both codes provide quasi-identical results in Cartesian geometry. Test 1-b shows that, for both codes, four nodes per assembly are necessary to reach a precision under 1%. It also shows an expected influence from the embedded ADFs on the power of the central assembly for both codes: ADFs increase the difference of flux level between two adjacent calculation meshes since they enable simulation of flux discontinuity at meshes interfaces [8]. These results also demonstrate that the FA ADFs are correctly implemented in the cross-sections and do not increase the difference between NEM and CRONOS predictions.

Figure 5.4. Normalised power and k_{eff} results of Test 1-a

Comparison of K_{eff}

	CRONOS	NEM	Rel. diff. %
1 node / FA	1.06892	1.06917	-0.023
4 nodes / FA	1.06894	1.06896	-0.002

One node per assembly

1.0640 1.0607 0.31	1.0110 1.0165 -0.54	1.0640 1.0607 0.31
1.0110 1.0165 -0.54	0.6991 0.6912 1.14	1.0110 1.0165 -0.54
1.0640 1.0607 0.31	1.0110 1.0165 -0.54	1.0640 1.0607 0.31

Four nodes per assembly

1.0640 1.0640 0.00	1.0110 1.0114 -0.04	1.0640 1.0640 0.00
1.0110 1.0114 -0.04	0.6981 0.6985 -0.06	1.0110 1.0114 -0.04
1.0640 1.0640 0.00	1.0110 1.0114 -0.04	1.0640 1.0640 0.00

1.064	CRONOS
1.06395	NEM
0.00	Rel. Diff. %

Figure 5.5. Normalised power and k_{eff} results of Test 1-b

Comparison of K_{eff}	CRONOS	NEM	Rel. diff. %
1 node / FA	1.06700	1.06741	-0.038
4 nodes / FA	1.06712	1.06714	-0.002

One node per assembly

1.0640 1.0594 0.43	0.9985 1.0075 -0.89	1.0640 1.0594 0.43
0.9985 1.0075 -0.89	0.7513 0.7325 2.57	0.9985 1.0075 -0.89
1.0640 1.0594 0.43	0.9985 1.0075 -0.89	1.0640 1.0594 0.43

Four nodes per assembly

1.0630 1.0631 -0.01	1.0010 1.0012 -0.02	1.0630 1.0632 -0.01
1.0010 1.0012 -0.02	0.7431 0.7427 0.05	1.0010 1.0012 -0.02
1.0630 1.0632 -0.01	1.0010 1.0012 -0.02	1.0630 1.0631 -0.01

1.0630	CRONOS
1.0632	NEM
-0.01	Rel. Diff. %

Figure 5.6. Normalised power and k_{eff} results of Test 2-a

Comparison of K_{eff}	CRONOS	NEM	Rel. diff. %
1 node / FA	0.894695	0.901714	-0.778
4 nodes / FA	0.899507	0.900000	-0.055

One node per assembly

0.8133 0.8213 -0.97	1.1420 1.1410 0.09	0.8133 0.8213 -0.97
1.1420 1.1410 0.09	1.1780 1.1505 2.39	1.1420 1.1410 0.09
0.8133 0.8213 -0.97	1.1420 1.1410 0.09	0.8133 0.8213 -0.97

Four nodes per assembly

0.8216 0.8226 -0.12	1.1390 1.1389 0.01	0.8216 0.8226 -0.12
1.1390 1.1389 0.01	1.1570 1.1542 0.24	1.1390 1.1389 0.01
0.8216 0.8226 -0.12	1.1390 1.1389 0.01	0.8216 0.8226 -0.12

0.8216	CRONOS
0.8226	NEM
-0.12	Rel. Diff. %

Figure 5.7. Normalised power and k_{eff} results of Test 2-b

Comparison of K_{eff}	CRONOS	NEM	Rel. diff. %
1 node / FA	0.912827	0.912859	-0.004
4 nodes / FA	0.912802	0.912599	-0.022

One node per assembly

0.8543 0.8502 0.48	1.1070 1.1139 -0.62	0.8543 0.8502 0.48
1.1070 1.1139 -0.62	1.1550 1.1437 0.99	1.1070 1.1139 -0.62
0.8543 0.8502 0.48	1.1070 1.1139 -0.62	0.8543 0.8502 0.48

Four nodes per assembly

0.8538 0.8529 0.10	1.1100 1.1105 -0.05	0.8538 0.8530 0.10
1.1100 1.1105 -0.05	1.1470 1.1462 0.07	1.1100 1.1105 -0.05
0.8538 0.8529 0.10	1.1100 1.1105 -0.05	0.8538 0.8530 0.10

0.8538	CRONOS
0.8530	NEM
0.10	Rel. Diff. %

Test 2 (Figures 5.6. and 5.7.) shows that the change of boundary condition (change from reflective BC to zero flux BC) and the introduction of a thick reflector with realistic characteristics do not change the agreement of the codes, provided that both solutions are spatially converged. Once again the comparison of results with and without ADFs shows a common correct implementation of the ADFs into the cross-sections.

Test 3 (Figure 5.8.) shows that the change of geometry leads to noticeable discrepancies between NEM and CRONOS2. As cross-sections are the same as in Test 2 the origin of the discrepancies can be due to:

- The fact that the NEM results are not spatially converged:
  - Only one mesh per assembly is used by NEM for hexagonal geometries, but Test 2 proves that the NEM code is then not spatially converged and discrepancies between one node and four nodes per assembly can be of the order of 1% on the central assembly. Note that the CRONOS2 results presented for Test 3 are spatially converged.
- The fact that the NEM numerical method is less accurate in hexagonal geometry than it is in Cartesian geometry. Note that the CRONOS2 numerical method is unchanged for Cartesian and hexagonal geometry.

As NEM cannot increase the number of nodes per assembly in hexagonal geometry, it is currently impossible to separate the effect of the convergence from the one of the numerical method.

Figure 5.8. Normalised power and k_{eff} results of Test 3

Comparison of k_{eff}

	CRONOS 3 nodes / FA	NEM 1 node / FA	Rel. diff. %
with ADFs	0.863504	0.877433	-1.587
without ADFs	0.882087	0.889030	-0.781

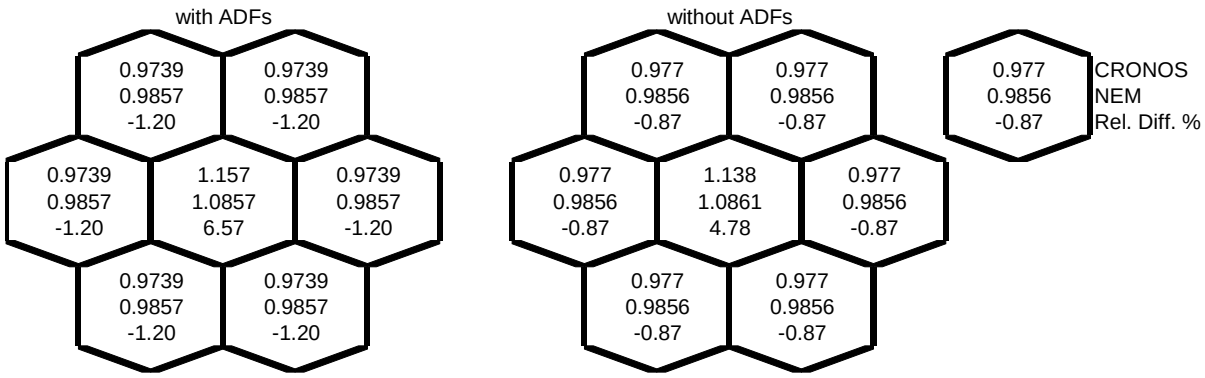

The comparison between Tests 4 and 5 (Figures 5.9. and 5.10.) shows that the physical nature of the reflector has an impact on the code behaviour. The PWR reflector contains less steel and more water; that changes its neutronic behaviour. It is worth taking a closer look at the different sets of reflector data (Table 2) used in the simple test problems in order to better understand the differences between them. It is another question to understand how the different codes are able to describe the neutron flux solution in the different reflector materials.

Figure 5.9. Normalised power and k_{eff} results of Test 4

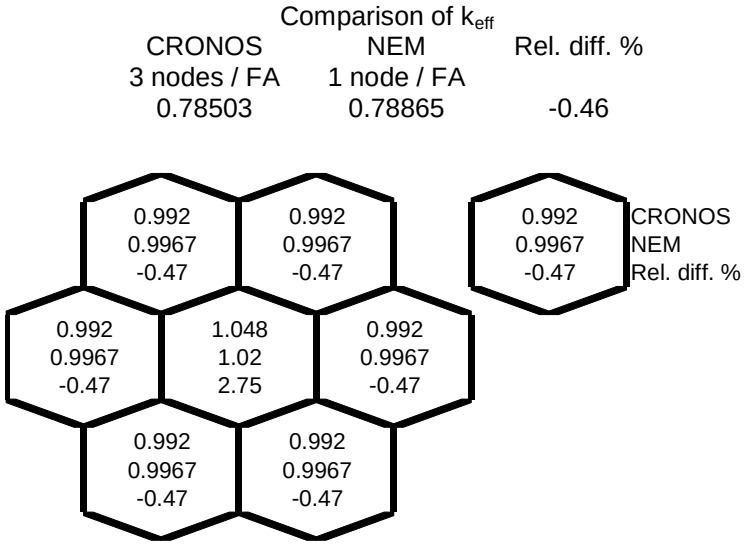

Figure 5.10. Normalised power and k_{eff} results of Test 5

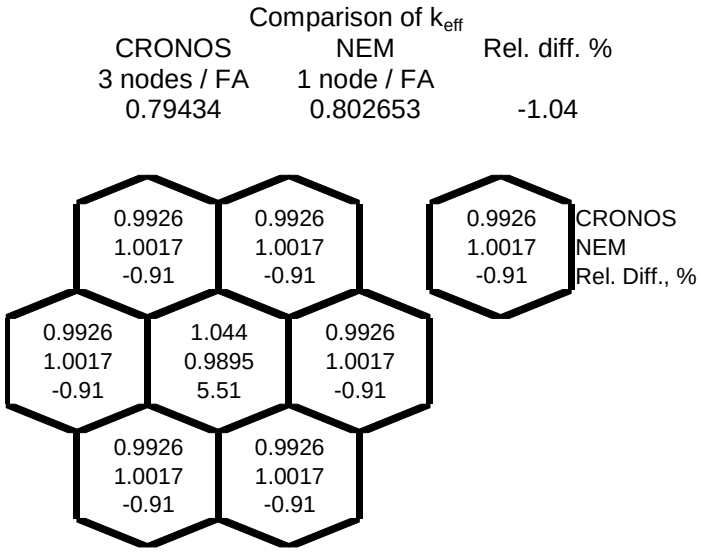

The point of view adopted here is to consider each given set of cross-sections for the reflector as representing a homogeneous medium in which an analytical (or fine mesh) solution is ultimately sought. Two types of neutronic properties of the medium are used to characterise the reflector. First, the migration of neutrons is characterised by the diffusion lengths in the fast and thermal groups (L_1 and L_2). These are defined by the formulae:

$$L_1^2 = \frac{D_1}{\Sigma_{a1} + \Sigma_{S1}} \quad \text{and} \quad L_2^2 = \frac{D_2}{\Sigma_{a2}} \tag{5.1}$$

Secondly, if the reflector is very thick and in plane geometry, then the elements of the albedo matrix (group-to-group neutron return probabilities) are uniquely determined by the diffusion properties of the reflector medium. The following formulae apply for two groups:

$$
\begin{aligned}
\alpha_{11} &= \frac{L_1 - 2D_1}{L_1 + 2D_1} \\
\alpha_{12} &= 0 \\
\alpha_{21} &= \frac{4L_1^{\,2}L_2^{\,2}\,\Sigma_{S1}}{(L_1 + 2D_1)(L_2 + 2D_2)(L_1 + L_2)} \\
\alpha_{22} &= \frac{L_2 - 2D_2}{L_2 + 2D_2}
\end{aligned}
\tag{5.2}
$$

The values of the above quantities are shown in Table 5.4. An examination of these results demonstrate the following tendencies: there are no differences in the diffusion lengths with ADFs (Case 1) or without ADFs (Case 2); the albedos are all, at least, slightly better in Case 1 than in Case 2; this is in line with the fact that both CRONOS2 and NEM calculate a lower k_{eff} with ADFs, albeit by differing amounts; there is a large difference in the purely thermal neutron albedo (α_{22}); finally, this may correlate with the differing predictions for the change in k_{eff} produced by the two codes. Again, this points in the direction of inadequately describing the thermal neutron flux behaviour near the core-reflector interface.

Table 5.4. Neutronic properties of the two different reflector materials

	HELIOS data without ADFs for VVER (Case 1)	**HELIOS data with ADFs for VVER (Case 2)**	**CASMO data with ADFs for PWR (Case 3)**	**CASMO data with ADFs for VVER (Case 4)**
L_1 (cm)	7.76	7.76	6.10	8.26
L_2 (cm)	2.38	2.38	3.74	3.29
α_{11}	0.6291	0.6200	0.5042	0.6311
α_{12}	0.0000	0.0000	0.0000	0.0000
α_{21}	0.0551	0.0427	0.1160	0.0527
α_{22}	0.6162	0.2237	0.3029	0.2634

The properties of the PWR reflector (Case 3) are notably different from the VVER reflector (Case 2). This is probably due to more water and less steel in the reflector. The return of fast neutrons back to the core is reduced by comparison (α_{11}). This is a partial reason for the reduction in k_{eff} by some 10%. On the other hand, more of the fast neutrons return back to the core as thermal ones (α_{21}). This increases power peaking in the outermost fuel rods and causes flattening in the assembly-wise power distribution. These reasons enhance neutron leakage from the core as well. The VVER reflector albedos derived from CASMO-3 data (Case 4) agree reasonably with those derived from HELIOS data (Case 2), but they are influenced by clear differences in the diffusion lengths.

Analytical two-group diffusion theory for a non-multiplying homogeneous medium tells us that the solution in the reflector is expressed in terms of the shape function $\exp(\pm x/L_1)$, in both fast and thermal groups, and the shape function $\exp(\pm x/L_2)$ in the thermal group. Let us notice that L_2 is lower with the VVER reflector. That increases the thermal flux gradient in the reflector and gives harder work to the code and enhances code discrepancies.

It is important to underline the fact that the same method is used to solve the diffusion equation in hexagonal geometry in the PSU code NEM and in RELAP-3D (utilised by KU). This is the Nodal Expansion Method (NEM); it utilises a transverse integration procedure and represents the 1-D

transverse integrated flux with higher order (up to 4) polynomial expansion. When the transverse integration procedure is applied in the conventional manner in the hexagonal geometry, the resulting one-dimensional diffusion equations contain unphysical singular terms [7]. These complications originate from the fact that the surface of the hexagon does not align with the Cartesian axis. The Lawrence approach for addressing these difficulties is implemented in NEM, which is to simplify the singular terms and to use continuous but piece-wise differentiable polynomials to approximate the solutions of the singular diffusion equations. While this approach works relatively well for reactor cores with flux gradients that are not very steep and have small mesh sizes (in terms of the smallest neutron mean free path), its accuracy is degraded in the VVER-1000 core calculations. This is because the VVER-1000 reflector properties were found to increase flux gradients at the core/reflector interface. The difficulties in NEM with the Lawrence approach for hexagonal geometry treatment to handle high exponential flux gradients are thus highlighted more.

Let us notice that, while the flux gradients in the reflectors are the steepest ones, steep flux gradients can also be found in the VVER-1000 core when control rods are inserted. The inaccuracy of the NEM method, for both at core/reflector boundary and in the vicinity of control rods, can be overcome by implementing subdivision of the hexagonal nodes. The NEM method in hexagonal geometry, contrary to the NEM method in Cartesian geometry, does not allow for such a subdivision, thus limiting the accuracy of the method, especially for VVER-1000 cores, which have large assemblies in terms of minimum neutron mean free path (i.e. diffusion length). In order to improve the accuracy of the NEM method without subdivision of the hexagonal nodes, two enhancements are needed:

- An addition to the 4^{th} order NEM polynomial expansion analytical terms (exponential or hyperbolic functions) that would, thus, make the expansion semi-analytical, which will help model the steep flux gradients at the interfaces of unlike assemblies and core/reflector boundaries better.

- A correction of the approximations introduced by applying the transverse integration procedure in hexagonal geometry either by using a conformal mapping method or by avoiding transverse integration in a radial plane and directly solving 2-D diffusion equation.

In summary, performed sensitivity studies narrowed down the possible sources of the deviation to two. As was expected, the first contributor was revealed to be differences in the methods used in the different codes for solving the diffusion equation in hexagonal geometry. The second contribution was discovered to be the impossibility of NEM to reduce its mesh size in hexagonal geometry.

Chapter 6

CONCLUSION

The OECD/DOE/CEA V1000CT benchmark has been developed to provide a validation basis for the new generation best-estimate codes – coupled 3-D neutron-kinetics system thermal-hydraulic codes. Based on the previous experience, three benchmark exercises, which allow for a consistent and comprehensive validation process, were defined. In the first benchmark exercise the participants initialised their system models and tested the thermal-hydraulic system responses using specified point kinetics parameters. The purpose of Exercise 2 of the V1000CT-1 benchmark was to test the core neutronics response to imposed thermal-hydraulic boundary conditions and to initialise the participants' coupled 3-D core models. Completing the first two benchmark exercises will allow for a thorough examination of the coupled core/plant system transient modelling in Exercise 3 using the models developed in the first and second exercises. In the second exercise only the core and the vessel were modelled. Inlet and outlet core transient boundary conditions were provided. Exercise 2, discussed in this report, enabled participants to initialise and verify their models before focusing on the main objective of the benchmark – testing of coupling methodologies in terms of numerics, temporal and spatial mesh overlays. This benchmark was created to support the determination of the applicability of 3-D coupled thermal-hydraulics/neutron kinetics codes to safety analysis of VVER-1000 special transients. The benchmark is based on a real plant transient where one main coolant pump switches on while the other three pumps are in operation.

A detailed evaluation of the differences between the calculated results submitted by the participants and the plant measured data were presented in Chapter 4. The analyses of the results of Exercise 2 show that the participants' results for each parameter are in reasonable agreement. The explanation for some of the discrepancies in the participants' steady-state and transient results for Exercise 2 are the observed differences as reported in Table 4.1., participants' models and in the answers to the questionnaire given in Appendix B. Some of these differences are the utilisation of the provided boundary conditions as well as different core neutronics and thermal-hydraulic nodalisations and models.

During the second OECD/DOE/CEA V1000CT benchmark workshop conducted in Sofia, Bulgaria in April 2004 [6], it was discovered that two clusters of participants' results for normalised radial power distribution were formed for both HP-SS conditions and HZP conditions. The observed difference between these two clusters is in the range of ±11%, while the difference within each of the clusters is in the range of ±1.5%. Steps were taken to understanding this problem, and are described in Chapter 5. This chapter of the report showed the results and the observations of this study as well as its most important conclusions. In summary, sensitivity studies performed narrowed down the possible sources of the deviation to two. As it was expected the first contributor was revealed to be differences in the methods used in the different codes for solving the diffusion equation in hexagonal geometry. The second contribution was discovered to be the NEM's impossibility to reduce its mesh size in hexagonal geometry.

From the results presented in this report it can be concluded that all the codes are capable of modelling the transient “MCP switching on when the other three pumps are in operation” in a VVER-1000 system. Deviations of the steady-state and transient results from the reference do occur, generally due to the manner in which the boundary conditions are used, and differences in nodalisation.

Overall, this benchmark has been well accepted internationally, with nine organisations representing eight countries participating in the second exercise of the benchmark. The results submitted by the participants for Exercise 2 were used to prepare the code-to-code comparisons with the subsequent statistical analyses. The results of this exercise enabled participants to initialise and verify their coupled 3-D neutron-kinetics core thermal-hydraulics boundary conditions models, which in turn is very important for conducting a correct assessment of the performance of the coupled codes in the last exercise of the benchmark.

REFERENCES

[1] Ivanov, K., P. Groudev, R. Gencheva,B. *Ivanov,Letter-Report on Kozloduy NPP Transient*, US DOE, September 2000.

[2] Ivanov, K., *et al*., *PWR MSLB Benchmark. Volume 1: Final Specifications*, NEA/NSC/DOC(99)8, April 1999.

[3] Solis, J., *et al.*, *Boiling Water Reactor Turbine Trip (TT) Benchmark Volume I: Final Specifications*, NEA/NSC/DOC(2001)1, June 2001.

[4] Ivanov, B., K. Ivanov, P. Groudev, M. Pavlova, V. Hadjiev, *VVER-1000 Coolant Transient Benchmark (V1000-CT). Phase 1 – Final Specification*, NEA/NSC/DOC(2002)6.

[5] Kuntz, R.F., G.F. Kasmala, J.H. Mahaffy, *Automated Code Assessment Program: Technique Selection and Mathematical Prescription*, Applied Research Laboratory, Pennsylvania State University, Letter Report 3 to US NRC, April 1998.

[6] *OECD/DOE/CEA VVER-1000 Coolant Transient Benchmark. Summary of the 2nd Workshop (V1000-CT2)*, Sofia, Bulgaria, 5-6 April 2004, NEA/NSC/DOC(2004)9.

[7] Ivanov, B., S. Aniel, P. Siltanen, E. Royer, K. Ivanov, "Impact of Cross-section Generation Procedures on Simulation of VVER-1000 Pump Startup Experiment in the OECD/DOE/CEA V1000CT Benchmark by Coupled 3-D Thermal-hydraulics Neutron Kinetics Models", *Prog. in Nuclear Energy*, Vol. 48, No. 8, pp. 746-763 (2006).

[8] Smith, K., "Assembly Homogenisation Techniques for Light Water Reactor Analysis", *Prog. in Nuclear Energy*, 17, No. 3, pp. 303-335 (1986).

[9] Lee, J., N.Z. Cho, "AFEN Method and its Solutions of the Hexagonal Three-dimensional VVER-1000 Benchmark Problem", *Prog. in Nuclear Energy*, Vol. 48, No. 8, pp. 880-890 (2006).

[10] Akherraz, B., A.M. Baudron, J.J. Lautard, C. Magnaud, F. Moreau, D. Schneider, M. Gonzales, *Manuel de Référence CRONOS 2.6*, Technical Report SERMA/LENR/RT/04-3433/A, CEA.

[11] Grundmann, U., S. Mittag, U. Rohde, *DYN3D Version 3.1 (FORTRAN90) – Code for Calculation of Transients in Light Water Reactors (LWR) with Hexagonal or Quadratic Fuel Elements, Code Manual and Input Data Description for Release*, Forschungszentrum Rossendorf, Germany, November 2003.

[12] KyrkiRajamäki R., *Three-dimensional Reactor Dynamics Code for VVER Type Nuclear Reactors*, Technical report 246, DrTech thesis, Technical Research Centre of Finland (1995).

[13] Joo, H.G., D. Barber, G. Jiang, T. Downar, *PARCS: A Multidimensional Two-group Reactor Kinetics Code Based on the Nonlinear Analytical Nodal Method*, PARCS Manual Version 2.20, Purdue University, School of Nuclear Engineering, July 2002.

[14] *RELAP5-3D Code Manuals: Volume I: Code Structure, System Models and Solution Methods; Volume II: User's Guide and Input Requirements; Volume IV: Models and Correlations; Volume V: User's Guidelines*, INEEL-EXT-98-00834, Revision 1.3a, February 2001.

[15] Ivanov, K., *et al*, "Features and Performance of a Coupled Three-dimensional Thermal-hydraulics/ Kinetics Code TRAC-PF1/NEM PWR Analysis Code," *Ann. Nucl. Energy*, 26, 1407 (1999).

[16] Schnurr, N.M., R.G. Steinke, V. Martinez, J.W. Spore, *TRAC-PF1/MOD2. Volume II. User's Guide*.

Appendix A

DESCRIPTION OF CODES

COREDAX (KAIST)

The COREDAX code is a hexagonal-z three-dimensional diffusion nodal code. It is based on the analytic function expansion nodal method (AFEN) and consists of several unique features: i) implementation of the AFEN method that employs no transverse integration and that represents the solution in terms of analytic solution bases, ii) inclusion of transverse gradient basis functions, iii) use of interface flux moments, iv) implementation of the coarse group rebalance (CGR) acceleration scheme and v) kinetics calculation capability based on the solution decomposition [9].

CRONOS2 (CEA)

CRONOS2 utilises the Finite Element Method (FEM), which is based on less regular solutions and it uses the weak formulation of the diffusion equation: The FEM is based on a discrete approximation of the various functional spaces involved by the general weak formulation [10]. The CRONOS2 hexagonal calculations are often done using the standard parabolic Lagrangian finite elements with 19, 61 or 127 nodes per hexagon (depending on whether the hexagons are divided in 1, 2 or 3 calculation meshes).

DYN3D (FZR, NRI)

DYN3D is a three-dimensional core model for dynamic and depletion calculations in LWR cores with quadratic or hexagonal fuel assembly geometry [11]. The neutron-kinetic model is based on the solution of the three-dimensional, two-group neutron diffusion equations by nodal expansion methods. Different methods are used for quadratic and hexagonal fuel assembly geometry. In the case of Cartesian geometry, the three-dimensional diffusion equation of each node is transformed into three one-dimensional equations for each direction (x, y, z) by transversal integrations. The equations are coupled by the transversal leakage term. In each energy group, the one-dimensional equations are solved with the help of flux expansions in polynomials up to second order and exponential functions are the solutions of the homogeneous equation. The fission source in the fast group and the scattering source in the thermal group as well as the leakage terms are approximated by the polynomials. In the case of hexagonal fuel assemblies, the diffusion equation in the node is transformed into a two-dimensional equation in the hexagonal plane and a one-dimensional equation in the axial direction. The two equations are coupled by the transverse leakage terms that are approximated by polynomials up to the second order. Considering the two-dimensional equation in the hexagonal plane, the side-averaged values (HEXNEM1) or the side-averaged + corner-point values (HEXNEM2) of flux and current are used for the approximate solution of the diffusion equation.

HEXTRAN (VTT)

The three-dimensional core neutronics, heat transfer and thermal-hydraulics solution method of the HEXTRAN code is based on coupling and extension of the steady-state hexagonal core simulator and the one-dimensional thermal-hydraulics code [12].

The two-group neutron diffusion equations are solved in HEXTRAN by a nodal expansion method in x-y-z geometry within the reactor core. A basic feature of the method is decoupling of the two-group equations into separate equations for two spatial modes and reconstruction of group fluxes from characteristic solutions to these equations. The two solutions are called the fundamental or asymptotic mode, which have a fairly smooth behaviour within a homogenised node, and the transient mode, which deviates significantly from zero only near material discontinuities. The nodal equations are solved with a two-level iteration scheme where only one unknown per node, the average of fundamental mode, is determined in inner iterations. The nodal flux shapes are improved in outer iterations by recalculation of the coupling coefficients.

The thermal-hydraulic calculation of the reactor core is performed in parallel to one-dimensional hydraulic channels, each channel usually coupled with one fuel assembly. The channels can be further divided into axial sub-regions, to take into account the geometric, hydraulic and heat transfer characteristics of the fuel bundles. Parallel to the heated channels, several unheated bypass channels can be modelled. Channel hydraulics is based on conservation equations for steam and water mass, total enthalpy and total momentum, and on a selection of optional correlations describing, for example, slip, non-equilibrium evaporation and condensation and one- and two-phase friction. The phase velocities are related to one another by an algebraic slip ratio or by the drift flux formalism. The thermal-hydraulic solution methods are the same as in the one-dimensional code TRAB.

During the hydraulic iterations, a one-dimensional heat transfer calculation is made for an average fuel rod of each assembly. The radial heat conduction of the fuel rod is solved according to Fourier's law. The fission power is divided into prompt and delayed power parts and a fraction of the power can be dissipated into heat directly in the coolant. Decay heat is included in the thermal power.

Advanced time integration methods are applied in the dynamic calculation. The numerical technique can vary between the standard fully implicit theta method and the central-difference theta method both in the heat conduction calculation for fuel rods and in the solution of thermal-hydraulic conservation equations for cooling channels.

HEXTRAN is a best-estimate code. Possibilities to modify the neutronics parameters have been included in the code so that the conservative nature of the calculations can be simply and reliably modified without changing the ordinary neutronics data.

RELAP5/PARCS (FZK, UPISA)

The transient neutron kinetic response of the core is simulated by the core simulator PARCS version 2.5, which is coupled to RELAP5 via PVM. PARCS solves time-dependent neutron diffusion equations for up to six energy groups using the triangular polynomial expansion (TPEN) method [13].

RELAP5-3D (KU)

NESTLE, the multi-dimensional neutron kinetics model in RELAP5-3D was developed to allow the user to model reactor transients where the spatial distribution of the neutron flux changes with time [14]. The neutron kinetics model uses the few-group neutron diffusion equations. Two or four energy groups can be utilised, with all groups being thermal groups (i.e. upscatter exits) if desired. Core geometries modelled include Cartesian and hexagonal. Three-, two- and one-dimensional models can be utilised. Various core symmetry options are available, including quarter, half and full core for Cartesian geometry and one-sixth, one-third and full core for hexagonal geometry. Zero flux, non-re-entrant current, reflective and cyclic boundary conditions are treated. The few-group neutron diffusion equations are spatially discretised utilising the Nodal Expansion Method (NEM). Quartic or quadratic polynomial expansions for the transverse integrated fluxes are employed for Cartesian or hexagonal geometries, respectively. Transverse leakage terms are represented by a quadratic polynomial or constant for Cartesian or hexagonal geometry, respectively. Discontinuity factors (DFs) are utilised to correct for homogenisation errors. Transient problems utilise a user-specified number of delayed neutron precursor groups. The neutron kinetics subroutines require input regarding the neutron cross-sections in the computational nodes of the kinetics mesh. A neutron cross-section model was implemented. It allows the neutron cross-sections to be parameterised as functions: heat structure temperatures, fluid void fraction or fluid density, poison concentration and fluid temperatures. A flexible coupling scheme between the neutron kinetics mesh and the thermal-hydraulics mesh has been developed to minimise the input data needed to specify the neutron cross-sections in terms of thermal-hydraulic variables. A control rod model has been implemented so that the effect of the initial position and subsequent movement of the control rods during transients may be taken into account in the computation of the neutron cross-sections.

TRAC-PF1/NEM (PSU)

NEM (Nodal Expansion Method) is a 3-D multi-group nodal code developed at PSU for modelling both steady-state and transient core conditions [15]. It utilises a transverse integration procedure and is based on the partial current formulation of the nodal balance equations. The code has options for modelling of 3-D Cartesian, cylindrical and hexagonal geometry. The utilisation of NEM in hexagonal geometry introduces several complications not encountered for Cartesian geometry. These complications originate form the fact that the surface of the hexagon does not align with the Cartesian axis. The Lawrence approach (Lawrence, 1983) for addressing these difficulties is implemented in the NEM code. The NEM code is coupled to the Transient Reactor Analysis Code (TRAC), which is an advanced best-estimate system code for analysing light water reactor (LWR) accidents. This code has been developed at the Los Alamos National Laboratory under the sponsorship of the Reactor Safety Research Division of the US Nuclear Regulatory Commission (NRC) [16]. The code has the following features: a one- or three-dimensional treatment of the pressure vessel and its associated internals, a two-fluid, non-equilibrium hydrodynamics model with a non-condensable gas field and a solute tracking, a flow-regime dependant constitutive equation treatment, an optional re-flood tracking capability for bottom-flood and falling-film quench fronts and a consistent treatment of entire accident sequences, including the generation of consistent initial conditions.

Appendix B

ANSWERS TO THE EXERCISE 2 QUESTIONNAIRE

CEA

I. Thermal-hydraulic core model

1. *Core thermal hydraulic (TH) model and nodalisation (1-D, 3-D and number of TH channels or cells). How are the channels/TH cells chosen?*

   Model: 3-D, number of TH channels: 163 (1 per fuel or reflector assembly).

2. *Core TH axial nodalisation?*

   Four (4) nodes in the bottom reflector, 12 nodes in the active part, 3 nodes in the top reflector.

3. *Number of heat structures (fuel rods) modelled?*

   Number of heat structures (fuel rods) modelled: 163 (1 per TH channel).

4. *What is the radial and axial heat structure (fuel rod) nodalisation?*

   Radial nodalisation: 8 meshes in the fuel, 6 meshes in the clad; axial nodalisation: channels axial meshing.

5. *What is the relation used for Doppler temperature?*

   The one defined in the benchmark specifications.

6. *Used correlations for fuel properties vs. temperature?*

   The ones defined in the benchmark specifications.

II. Core neutronics model

1. *Numerical method used?*

   Finite Element Method.

2. *Number of radial neutronics nodes per assembly?*

   Two (2) nodes per assembly (61 mesh points).

3. *What is the number of axial layers used?*

   Physical nodes: 12 (10 in the active part 1 for each axial reflector) with 2 nodes per physical node.

4. *How are the radial and axial reflectors modelled?*

   Reflectors modelled with the cross-sections given in the benchmark specifications.

5. *Spatial decay heat distribution modelling?*

   The spatial decay heat is included in FLICA4 by adding the residual power value to the total power. The spatial decay heat distribution is thus the same as the fission power distribution.

6. *What is the cross-section interpolation procedure used?*

   CRONOS2 one, that has been tested to give the same results as the interpolation procedure given as benchmark specification.

7. *What is the method used to get a critical reactor at the beginning of the transient?*

   Fission matrix normalisation by the steady-state eigenvalue.

III. Coupling schemes

1. *Hydraulics/heat structure spatial mesh overlays (mapping schemes in a radial axial plane)?*

   The meshing is coherent since there is one heat structure per TH channel and the axial meshing of the heat structures correspond to the TH axial meshing.

2. *Hydraulics/neutronics spatial mesh overlays (mapping schemes in a radial axial plane)?*

   The radial and axial meshing are coherent.

3. *Heat structure/neutronics spatial mesh overlays (mapping schemes in a radial axial plane)?*

   As a consequence of the answers to questions one and two, the radial and axial meshing are coherent.

4. *Coupling numerics – explicit, semi-implicit or implicit?*

   Explicit coupling.

5. *Coupling type – external or internal?*

   External.

6. *Coupling design – serial integration or parallel processing?*

   Serial integration.

IV. General

1. *Deviations from the updated Final Specification?*

   None.

2. *User assumptions?*

   Decay heat with the same distribution as the fission power one.

3. *Specific features of the codes used?*

   Full 3-D TH/neutronic coupling.

FZK

I. Thermal-hydraulic core model

1. *Core thermal hydraulic (TH) model and nodalisation (1-D, 3-D and number of TH channels or cells). How are the channels/TH cells chosen?*

   In the 1-D core model, the thermal-hydraulics cells were chosen as recommended in the Specifications, i.e. based on the TRAC-nodalisation of the reference run. Hence, the core consists of 18 parallel channels and one bypass channel. No cross-flow is considered between these parallel channels since the coolant flow rate is high.

2. *Core TH axial nodalisation?*

   Axially the thermal-hydraulic channels consist of 12 axial elevations, 10 in the core region and two for the upper and lower reflector.

3. *Number of heat structures (fuel rods) modelled?*

   In total, 19 heat structures are included in the model, 18 representing the different fuel assembly groups that belong to a channel according to the mapping scheme as proposed in the specifications. The other heat structure represents the radial reflector.

4. *What is the radial and axial heat structure (fuel rod) nodalisation?*

   Each heat structure representing a number of fuel rods is divided in the same manner as in Exercise 1, i.e. in 10 radial nodes (6 in the fuel, 1 gap and 3 in the clad). In axial direction, 10 nodes of equal size as the corresponding fluid channel nodes are represented in the model.

5. *What is the relation used for Doppler temperature?*

   According to the specifications the same relation used in Exercise 1 was applied here, i.e. a 30/70% split of the fuel pellet centreline and the fuel pellet surface is used to compute the Doppler temperature.

6. *Used correlations for fuel properties vs. temperature?*

   As given in specifications, i.e. the same ones used for Exercise 1.

II. Core neutronics model

1. *Numerical method used?*

   PARCS solves the multi-group time-dependent diffusion equations with assembly spatial discretisation for hexagonal geometries using the triangle-based polynomial nodal expansion method (TPEN).

2. *Number of radial neutronics nodes per assembly?*

   One node per assembly.

3. *What is the number of axial layers used?*

   In total, 12 axial nodes are considered: 10 nodes for the active core and 2 for the lower and upper axial reflector.

4. *How are the radial and axial reflectors modelled?*

   Each of the 48 radial reflector elements is modelled as a neutronic node in each of the 10 axial levels of the active zone. The axial reflector is modelled by two axial reflector levels, one on the bottom and the other on core top.

5. *Spatial decay heat distribution modelling?*

   PARCS uses a simplified decay heat model with six groups of decay heat precursor (similar to the delayed neutron precursor equation) resulting in a node-wise solution of the precursor equation. Thus, in each time step the decay heat is obtained and summed with the fission power in order to determine the total power generated in each node.

6. *What is the cross-section interpolation procedure used?*

   The PARCS multi-dimensional interpolation scheme was used for the cross-section update during the transient calculations.

7. *What is the method used to get a critical reactor at the beginning of the transient?*

   Before the transient calculation starts, the fission source ($\nu\Sigma_f$) is adjusted with the effective multiplication factor.

III. Coupling schemes

1. *Hydraulics/heat structure spatial mesh overlays (mapping schemes in a radial axial plane)?*

   The radial mapping proposed in the specifications was adopted for the RELAP5/PARCS investigations, that is to say 18 heat structures and 18 fluid channels in the core with equal axial node size.

2. *Hydraulics/neutronics spatial mesh overlays (mapping schemes in a radial axial plane)?*

   One hydraulic node is used for each axial neutronic node. In the radial plane, 18 fluid channels are mapped over the 163 fuel assemblies (neutronic node) according to specifications.

3. *Heat structure/neutronics spatial mesh overlays (mapping schemes in a radial axial plane)?*

   The 163 fuel assemblies (PARCS neutronic nodes) are mapped according to the 18 heat structures in the RELAP5-model. The 48 radial reflector assemblies are similarly mapped to the heat structure 19. Axially, a one-to-one mapping between the heat structures and the respective neutronic nodes was implemented.

4. *Coupling numerics – explicit, semi-implicit or implicit?*

   Explicit coupling.

5. *Coupling type – external or internal?*

   An internal coupling scheme is implemented in RELAP5/PARCS. In the time domain, RELAP5 determines the time step size. RELAP5 updates the conduction, first and the hydraulics solution, second. The new thermal-hydraulics parameters are passed to PARCS to update the neutronic solution. The predicted new power distribution is passed back to RELAP in order to update the conduction and hydraulics solution for the next time step.

6. *Coupling design – serial integration or parallel processing?*

   The RELAP5/PARCS runs in a serial mode, where PVM facilitates only the interface for passing data between RELAP5 (process 1) and PARCS (process 2).

IV. General

1. *Deviations from the updated final specifications?*

   Use of the own PARCS-interpolation routine.

2. *User assumptions?*

   None.

3. *Specific features of the codes used?*

   None.

FZR

I. Thermal-hydraulic core model

1. *Core thermal hydraulic (TH) model and nodalisation (1-D, 3-D and number of TH channels or cells). How are the channels/TH cells chosen?*

   One-dimensional (1-D) TH model of the core with 24 channels, including 6 radial reflector TH channels (see *V1000CT-1* specification, Figure 3.2.1, p. 50).

2. *Core TH axial nodalisation?*

   Twelve (12) axial TH nodes (including 2 axial reflector zones).

3. *Number of heat structures (fuel rods) modelled?*

   Eighteen (18).

4. *What is the radial and axial heat structure (fuel rod) nodalisation?*

   Five (5) radial and 10 axial zones in fuel.

5. *What is the relation used for Doppler temperature?*

   Doppler temperature = volume averaged nodal temperature of fuel.

6. *Used correlations for fuel properties vs. temperature?*

   DYN3D correlations for VVER fuel properties.

II. Core neutronics model

1. *Numerical method used?*

   Nodal expansion method (NEM).

2. *Number of radial neutronics nodes per assembly?*

   One (1) node per assembly.

3. *What is the number of axial layers used?*

   Twelve (12).

4. *How are the radial and axial reflectors modelled?*

   Two (2) axial reflectors (lower and upper), 6 radial reflector zones.

5. *Spatial decay heat distribution modelling?*

   The DYN3D spatial decay heat distribution model is used.

6. *What is the cross-section interpolation procedure used?*

   Bilinear interpolation.

7. *What is the method used to get a critical reactor at the beginning of the transient?*

   Dividing the multiplication cross-sections by K_{eff}.

III. Coupling schemes

1. *Hydraulics/heat structure spatial mesh overlays (mapping schemes in a radial axial plane)?*

   Eighteen (18) radial zones for fuel TH channels/heat structures + 6 radial reflector zones, 12 axial zones in fluid channels (including reflector) and 10 axial zones in heat structures.

2. *Hydraulics/neutronics spatial mesh overlays (mapping schemes in a radial axial plane)?*

   In a radial plane: 24 hydraulic nodes and 211 neutronic nodes (with a radial reflector).In an axial plane: 12 hydraulic nodes and 12 neutronic nodes (with an axial reflector).

3. *Heat structure/neutronics spatial mesh overlays (mapping schemes in a radial axial plane)?*

   In a radial plane: 18 heat structure nodes and 163 neutronic nodes (without radial reflector nodes). In an axial plane: 10 heat structure nodes and 10 neutronic nodes (without axial reflector nodes).

4. *Coupling numerics – explicit, semi-implicit or implicit?*

   Explicit.

5. *Coupling type – external or internal?*

   Internal.

6. *Coupling design – serial integration or parallel processing?*

   Serial integration.

IV. General

1. *Deviations from the updated final specifications?*

   Relation for Doppler temperature (see I.5); Fuel, cladding, and fuel rod gap properties (see I.6).

2. *User assumptions?*

   None.

3. Specific features of the codes used?

   None.

KAIST

I. Thermal-hydraulic core model

1. *Core thermal hydraulic (TH) model and nodalisation (1-D, 3-D and number of TH channels or cells). How are the channels/TH cells chosen?*

   One-dimensional (1-D) TH model, 163 radial X and 12 axial TH cells (single channel per cell).

2. *Core TH axial nodalisation?*

   Twelve (12) nodes with the same axial size.

3. *Number of heat structures (fuel rods) modelled?*

   One (1) fuel rod per assembly.

4. *What is the radial and axial heat structure (fuel rod) nodalisation?*

   Twelve (12) axial nodes; 10 radial nodes (5: fuel; 5: cladding).

5. *What is the relation used for Doppler temperature?*

   $T_f = (1 - \alpha)T_{f,c} + \alpha T_f$ (where $\alpha = 0.7$).

6. *Used correlations for fuel properties vs. temperature?*

   Cross-section interpolation using data in benchmark specifications.

II. Core neutronics model

1. *Numerical method used?*

   Analytic Function Expansion Nodal (AFEN) Method.

2. *Number of radial neutronics nodes per assembly?*

   One (1) node per assembly.

3. *What is the number of axial layers used?*

   Twelve (12) axial layers.

4. *How are the radial and axial reflectors modelled?*

   Same as fuel assembly.

5. *Spatial decay heat distribution modelling?*

   Not considered.

6. *What is the cross-section interpolation procedure used?*

   Interpolation procedure provided from the benchmark team.

7. *What is the method used to get a critical reactor at the beginning of the transient?*

   $\Sigma/k_{eff.}$

III. Coupling schemes

1. *Hydraulics/heat structure spatial mesh overlays (mapping schemes in radial axial plane)?*

   One-hundred-and-sixty-three (163) radial/12 axial spatial meshes for both hydraulics and heat (one mesh per assembly).

2. *Hydraulics/neutronics spatial mesh overlays (mapping schemes in a radial axial plane)?*

   One-hundred-and-sixty-three (163) radial/12 axial spatial meshes for both hydraulics and neutronics (one mesh per assembly).

3. *Heat structure/neutronics spatial mesh overlays (mapping schemes in a radial axial plane)?*

   One-hundred-and-sixty-three (163) radial/12 axial spatial meshes for both heat and neutronics (one mesh per assembly).

4. *Coupling numerics – explicit, semi-implicit or implicit?*

   Explicit.

5. *Coupling type – external or internal?*

   Internal.

6. *Coupling design – serial integration or parallel processing?*

   Serial integration.

IV. General

1. *Deviations from the updated Final Specifications?*

   None.

2. *User assumptions?*

   Uniform pressure in a reactor (no cross-flow).

3. *Specific features of the codes used?*

   Several unique features in 3-D neutronics (AFEN) calculation:

   - no transverse integration;
   - use of analytic basis functions, including transverse gradient basis functions;
   - use of interface flux moments;
   - implementation of the coarse group rebalance (CGR) acceleration scheme;
   - kinetics calculation capability based on the solution decomposition.

KU

I. Thermal-hydraulic core model

1. *Core thermal-hydraulic (TH) model and nodalisation (1-D, 3-D and number of TH channels or cells). How are the channels/TH cells chosen?*

   Three-dimensional (3-D) core thermal-hydraulic model is FA by FA model with each fuel assembly mapped to a corresponding thermal-hydraulic channel, that is to say there are 163 thermal-hydraulic channels according to the quantity of fuel assemblies. The core thermal-hydraulic model also has a 6-sector core bypass (see hydraulics/heat structure spatial mesh overlays).

2. *Core TH axial nodalisation?*

   The core thermal-hydraulic axial nodalisation has 10 axial layers (mesh intervals 0.355 m) for fuel assemblies and radial reflector and also 2 axial layers (mesh intervals 0.236 m) for bottom and top axial reflectors.

3. *Number of heat structures (fuel rods) modelled?*

   The quantity of FA heat structures corresponds to the quantity of FA hydraulic channels, in other words, 163 FA heat structures correspond to 163 FA hydraulic channels.

4. *What is the radial and axial heat structure (fuel rod) nodalisation?*

   The axial heat structure nodalisation of fuel rod has 10 axial layers with the same axial mesh intervals (0.355 m) and radial four nodes in the fuel and four nodes in the cladding.

5. *What is the relation used for Doppler temperature?*

   In reactivity feedback calculations, the Doppler temperature is the fuel region average temperature, i.e. the average volume temperature computation of the fuel pin heat structure, in which the temperatures of gas gap and cladding regions are excluded.

6. *Used correlations for fuel properties vs. temperature?*

   The used thermal conductivity and volumetric heat capacity of uranium dioxide (UO_2) versus temperature are in Table 3.3.1, “Properties of fuel”, of the specification.

II. Core neutronics model

1. *Numerical method used?*

   The RELAP5-3D code multi-dimensional neutron kinetics model is based on the NESTLE code. This kinetics model solves the few-group neutron diffusion equations utilising the Nodal Expansion Method (NEM). Core geometry used in the RELAP5-3D analysis is hexagonal.

2. *Number of radial neutronics nodes per assembly?*

   The number of radial neutronics nodes per assembly is one. The Nodal Expansion Method cannot reduce its mesh size in hexagonal geometry.

3. *What is the number of axial layers used?*

   The core neutronics model has 10 axial layers (mesh intervals 0.355 m) for fuel assemblies and radial reflectors and 2 axial layers (mesh intervals 0.236 m) for bottom and top reflectors.

4. *How are the radial and axial reflectors modelled?*

   The radial reflector has 10 axial layers (mesh intervals 0.355 m) as a fuel assembly model. Bottom and top reflectors each have one axial layer (mesh interval 0.236 m).

5. *Spatial decay heat distribution modelling?*

   The decay heat model developed for the point reactor kinetics model has been modified in RELAP5-3D code to compute the decay power for both the point reactor kinetics model and for the multi-dimensional neutron kinetics model. Decay power is generated as the fission products undergo radioactive decay. The spatial decay heat distribution is carried out according to the contribution of the node into the total fission rate. The decay power model based on the ANS-79 decay heat standard was selected according to the specification's recommendation.

6. *What is the cross-section interpolation procedure used?*

   The cross-section interpolation procedure, presented in the subroutine lint4dm.f was used.

7. *What is the method used to get a critical reactor at the beginning of the transient?*

   The type of simulation to get a critical reactor at the beginning of the transient is RELAP5-3D STDY-ST problem option. The general form of the steady-state multi-group neutron diffusion equation, written in the standard form of the eigenvalue neutron diffusion equation, is used by this problem option.

III. Coupling schemes

1. *Hydraulics/heat structure spatial mesh overlays (mapping schemes in a radial axial plane)?*

   The volume and heat structure used to define sets of average thermal-hydraulic properties of the neutronics nodes is called a zone in the RELAP5-3D code. The user defines a number of zones (zone average thermal-hydraulic properties) for the computation of the neutron cross-sections in each node of the reactor core through the use of zone figures. A zone figure specifies which zone is to be used for the computation of the neutron cross-sections for each node in an axial plane of the reactor. Zone figures are required for each axial plane in the reactor model. Used RELAP5-3D core model is FA by FA (163 hydraulic channels and 163 heat structures) and the hydraulics/heat structure spatial mesh overlays (mapping schemes in a radial axial plane) are similar to the hydraulics/neutronics spatial mesh overlays.

2. *Hydraulics/neutronics spatial mesh overlays (mapping schemes in a radial axial plane)?*

   These mapping schemes in a radial axial plane can be described in the following way: the so-called coupling scheme between a thermal-hydraulic model and neutron kinetic model in an axial direction; bottom and top axial reflectors (layers 1 and 12) of the neutronics model are respectively bottom and top axial reflectors of the thermal-hydraulic model (layers 1 and 12); 10 layers of reactor core and radial reflector of the neutronics model (2^{nd} to 11^{th} layers) correspond to 10 layers of reactor core of the thermal-hydraulic model (2^{nd} to 11^{th} layers).

   The so-called radial coupling scheme between a thermal-hydraulic model and a neutron kinetic model: bottom and top axial reflectors (layers 1 and 12) of the neutronics model are respectively bottom and top axial reflectors of the thermal-hydraulic model (layers 1 and 12); 163 FA (1 630 neutronic nodes) correspond to 163 thermal-hydraulic channels (1 630 thermal-hydraulic zones); 48 kinetics meshes of radial reflector correspond to 6 thermal-hydraulic channels; 211 kinetics meshes of bottom reflector correspond to 6 thermal-hydraulic zones; 211 kinetics meshes of top reflector correspond to 6 thermal-hydraulic zones.

3. *Heat structure/neutronics spatial mesh overlays (mapping schemes in a radial axial plane)?*

   These mapping schemes in a radial axial plane are similar to the hydraulics/neutronics spatial mesh overlays described above.

4. *Coupling numerics – explicit, semi-implicit or implicit?*

   The system model is solved numerically using a semi-implicit advancement scheme. For slowly varying, quasi-steady transient calculations the user can select an option for solving the system model using a nearly-implicit scheme, which allows violation of the material Courant limit. In general, the executive provides for four different types of coupling: explicit thermal-hydraulic, explicit reactor kinetics, explicit control system and semi-implicit thermal-hydraulics. These four types have been developed to fully exploit various aspects of the RELAP5-3D program. A flexible coupling scheme between the neutron kinetics mesh and the thermal-hydraulics mesh has been developed to minimise the input data needed to specify the neutron cross-sections in terms of RELAP5-3D thermal-hydraulic variables (see above).

5. *Coupling type – external or internal?*

   Internal.

6. *Coupling design – serial integration or parallel processing?*

   Serial integration.

IV. General

1. *Deviations from the updated Final Specifications*

   None; fuel, cladding and fuel rod gap properties (see I.6).

2. *User assumptions?*

   The specification has boundary conditions on an FA basis for inlet FA mass flows (file MASS_FLOWS.BC.Rev3.xls). Eighteen (18) channel boundary conditions for inlet coolant temperatures were transformed to FA inlet coolant temperatures (boundary conditions on an FA basis).

3. *Specific features of the codes used?*

   Since RELAP5-3D code does not perform pin power reconstruction the fixed pin peaking factor $Kk^{max} = 1.00$ is assumed in the RELAP5-3D analysis.

NRI

I. Thermal-hydraulic core model

1. *Core thermal hydraulic (TH) model and nodalisation (1-D, 3-D and number of TH channels or cells). How are the channels/TH cells chosen?*

   Solution 1: 24 coolant channels; the location of fuel assemblies in coolant channels corresponds to Figure 3.2.1 in the benchmark specification.

   Solution 2: 211 coolant channels: 163 coolant channels for the heated core part and 48 coolant channels for radial reflectors.

2. *Core TH axial nodalisation?*

   Twelve (12) axial layers (10 layers for heated core part (10 × 35.5 cm), 2 layers for lower (23.6 cm) and upper axial reflectors (23.6 cm).

3. *Number of heat structures (fuel rods) modelled?*

   Three-hundred-and-twelve (312) fuel rods (pins) per fuel assembly.

4. *What is the radial and axial heat structure (fuel rod) nodalisation?*

   Number of radial nodes along the fuel pellet: 5; number of radial nodes along the cladding radius: 1; number of axial nodes (along the fuel rod): 10.

5. *What is the relation used for Doppler temperature?*

   The average fuel nodal temperature is used as the Doppler temperature in each kinetic node.

6. *Used correlations for fuel properties vs. temperature?*

   The thermal conductivities and heat transfer coefficient in the gas gap between fuel and cladding are determined in the frame of the DYN3D model.

II. Core neutronics model

1. *Numerical method used?*

   A nodal expansion method for solving the two-group neutron diffusion equation in hex-y geometry.

2. *Number of radial neutronics nodes per assembly?*

   One (1) radial neutronic node per fuel assembly.

3. *What is the number of axial layers used?*

   Twelve (12) axial layers (10 layers for the heated core part (10 × 35.5 cm), 2 layers for lower (23.6 cm) and upper axial reflectors (23.6 cm).

4. *How are the radial and axial reflectors modelled?*

   Radial reflectors are treated as artificial reflector assemblies surrounding the core with neutronic properties taken from a distributed library. Axial reflectors are modelled as artificial upper and lower axial layers consisting of hexagonal nodes. The zero flux boundary conditions are modelled at the outer boundary of radial and axial reflectors. The reflector assemblies have the same distance between opposite faces of the hexagon as fuel assemblies.

5. *Spatial decay heat distribution modelling?*

   There is no possibility of using a benchmark specified decay heat curve in the code DYN3D. It has its own decay heat power calculation based on power history. Burn-up calculation with burn-up dependent X-S library is necessary.

   Solution 1: 24 coolant channels model – the constant decay heat power – integral average from a benchmark specified decay heat curve.

   Solution 2: 211 coolant channels model – DYN3D burn-up distribution given at different time steps of core history was taken from the Kozloduy-6 transient and calculated in the VALCO project. The VALCO project data covers both VALCO and V1000CT transients, which were conducted one after another during the same series of commissioning experiments on Kozloduy-6. The V1000CT experiment was conducted approximately 140 FPD earlier than the VALCO transient, so only the first ~30 FPD of the VALCO power history (~172 FPD) was used to calculate the initial decay power level of the V1000CT experiment. The calculated initial value of decay heat is close enough to the value specified by the benchmark team.

6. *What is the cross-section interpolation procedure used?*

   The subroutine lintp2.f was used. This is practically the same subroutine as subroutine lint4d.f.

7. *What is the method used to get a critical reactor at the beginning of the transient?*

   The critical state is achieved by dividing the multiplication cross-sections by k_{eff}.

III. Coupling schemes

1. *Hydraulics/heat structure spatial mesh overlays (mapping schemes in a radial axial plane)?*

   One type of fuel assembly from the point of its heat structure; the arrangement of fuel assemblies in coolant channels is described in point I.1. and III.2.

2. *Hydraulics/neutronics spatial mesh overlays (mapping schemes in a radial axial plane)?*

   Solution 1: 24 coolant channels; structure of fuel assemblies corresponds to Figure 3.2.1 of the benchmark specification.

   Solution 2: 211 coolant channels; 163 coolant channels for heated core part and 48 coolant channels for radial reflectors.

3. *Heat structure/neutronics spatial mesh overlays (mapping schemes in a radial axial plane)?*

   The same as in point III.2. One type of heat structure in neutronic node.

4. *Coupling numerics – explicit, semi-implicit or implicit?*

   Explicit.

5. *Coupling type – external or internal?*

   Internal.

6. *Coupling design – serial integration or parallel processing?*

   Serial integration.

IV. General

1. *Deviations from the updated final specifications?*

   Slightly different modelling of decay heat and Doppler temperature.

2. *User assumptions?*

   None.

3. *Specific features of the codes used?*

   None.

PSU

I. Thermal-hydraulic core model

1. *Core thermal-hydraulic (TH) model and nodalisation (1-D, 3-D and a number of TH channels or cells). How are the channels/TH cells chosen?*

   Three-dimensional (3-D) TH model of the core with 24 channels, including 6 radial reflector TH channels.

2. *Core TH axial nodalisation?*

   Twelve (12) axial TH nodes (including 2 axial reflector nodes).

3. *Number of heat structures (fuel rods) modelled?*

   Eighteen (18) rods in a radial plane and ten in an axial plane

4. *What is the radial and axial heat structure (fuel rod) nodalisation?*

   Eight (8) radial and ten axial nodes are used.

5. *What is the relation used for Doppler temperature?*

   As specified.

6. *Used correlations for fuel properties vs. temperature?*

   No.

II. Core neutronics model

1. *Numerical method used?*

   Nodal Expansion Method (NEM).

2. *Number of radial neutronics nodes per assembly?*

   One (1) node per assembly.

3. *What is the number of axial layers used?*

   Twelve (12).

4. *How are the radial and axial reflectors modelled?*

   Two (2) axial reflectors (lower and upper); 48 radial nodes at each axial level.

5. *Spatial decay heat distribution modelling?*

   As specified.

6. *What is the cross-section interpolation procedure used?*

   As specified.

7. *What is the method used to get a critical reactor at the beginning of the transient?*

   Dividing the fission source ($\nu\Sigma_f$) with the effective multiplication factor.

III. Coupling schemes

1. *Hydraulics/heat structure spatial mesh overlays (mapping schemes in a radial axial plane)?*

   The radial mapping proposed in the specifications was adopted. There are thus 18 heat structures and 18 TH channels in the core with equal axial node size.

2. *Hydraulics/neutronics spatial mesh overlays (mapping schemes in a radial axial plane)?*

   The 211 neutronics nodes are mapped to18 heat structures.

3. *Heat structure/neutronics spatial mesh overlays (mapping schemes in radial axial plane)?*

   In a radial plane: 18 heat structure nodes and 211 neutronic nodes. In an axial plane 10 heat structure nodes and 12 neutronic nodes.

4. *Coupling numerics – explicit, semi-implicit or implicit?*

   Explicit.

5. *Coupling type – external or internal?*

   Internal.

6. *Coupling design – serial integration or parallel processing?*

   Serial integration.

IV. General

1. *Deviations from the updated final specifications?*

   None.

2. *User assumptions?*

   None.

3. *Specific features of the codes used?*

   None.

UPISA

I. Thermal-hydraulic core model

1. *Core thermal-hydraulic (TH) model and nodalisation (1-D, 3-D and number of TH channels or cells). How are the channels/TH cells chosen?*

   One-dimensional (1-D) nodalisation based on 28 TH parallel channels plus one bypass channel based on the 28 different FA type (BU, enrichment) present in the core.

2. *Core TH axial nodalisation?*

   Twenty (20) active nodes plus 2 non-active nodes on the edges.

3. *Number of heat structures (fuel rods) modelled?*

   One (1) homogenised fuel rod per assembly.

4. *What is the radial and axial heat structure (fuel rod) nodalisation?*

   Twenty (20) axial nodes and 12 radial nodes.

5. *What is the relation used for Doppler temperature?*

   Weighting factor 0.7.

6. *Used correlations for fuel properties vs. temperature?*

   Tabulated properties in function of the temperature.

II. Core neutronics model

1. *Numerical method used?*

   PARCS TPEN method.

2. *Number of radial neutronics nodes per assembly?*

   One (1).

3. *What is the number of axial layers used?*

   Twenty-two (22).

4. *How are the radial and axial reflectors modelled?*

   The radial reflectors have the same dimension as the fuel assembly and the temperature of the coolant in the bypass. The lower and upper axial reflectors have the same dimension as the first axial neutronic node and then have the same temperature as the coolant of the lower and upper plenum, respectively.

5. *Spatial decay heat distribution modelling?*

   ANS-79 model.

6. *What is the cross-section interpolation procedure used?*

   Linear, according to the benchmark look-up tables.

7. *What is the method used to get a critical reactor at the beginning of the transient?*
   Iterative method according to the k_{eff} convergence.

III. Coupling schemes

1. *Hydraulics/heat structure spatial mesh overlays (mapping schemes in radial axial plane)?*
   One by one.
2. *Hydraulics/neutronics spatial mesh overlays (mapping schemes in radial axial plane)?*
   One by one in a radial direction and two hydraulic nodes per one neutronic node, axially.
3. *Heat structure/neutronics spatial mesh overlays (mapping schemes in a radial axial plane)?*
   One by one in a radial direction and two hydraulic nodes per one neutronic node, axially.
4. *Coupling numerics – explicit, semi-implicit or implicit?*
   Semi-implicit.
5. *Coupling type – external or internal?*
   Internal.
6. *Coupling design – serial integration or parallel processing?*
   Parallel.

IV. General

1. *Deviations from the updated final specifications?*
   None.
2. *User assumptions?*
   None.
3. *Specific features of the codes used?*
   None.

VTT

I. Thermal-hydraulic core model

1. *Core thermal-hydraulic (TH) model and nodalisation (1-D, 3-D and number of TH channels or cells). How are the channels/TH cells chosen?*

   One-dimensional (1-D), 163 channels, one channel/assembly.

2. *Core TH axial nodalisation?*

   Twenty (20) axial nodes of equal height.

3. *Number of heat structures (fuel rods) modelled?*

   One-hundred-and-sixty-three (163), one fuel rod/assembly.

4. *What is the radial and axial heat structure (fuel rod) nodalisation?*

   Twenty (20) axial nodes; radially fuel rod modelled with 7 points in pellet and 2 points in cladding.

5. *What is the relation used for Doppler temperature?*

   As specified on page 20 of the final specification.

6. *Used correlations for fuel properties vs. temperature?*

   As specified on pages 29-30 of the final specification.

II. Core neutronics model

1. *Numerical method used?*

   Nodal Expansion Method.

2. *Number of radial neutronics nodes per assembly?*

   One node/assembly.

3. *What is the number of axial layers used?*

   Twenty (20) axial nodes of equal height.

4. *How are the radial and axial reflectors modelled?*

   Reflector nodes not modelled. Albedo boundary conditions used.

5. *Spatial decay heat distribution modelling?*

   Time evolution of decay heat followed dynamically in each assembly. For axial distribution, the initial steady-state fission power distribution used through the transient.

6. *What is the cross-section interpolation procedure used?*

   Linear interpolation and extrapolation from tables.

7. *What is the method used to get a critical reactor at the beginning of the transient?*

   Number of neutrons from fission divided by calculated keff.

III. Coupling schemes

1. *Hydraulics/heat structure spatial mesh overlays (mapping schemes in radial axial plane)?*
   One-to-one.
2. *Hydraulics/neutronics spatial mesh overlays (mapping schemes in radial axial plane)?*
   One-to-one.
3. *Heat structure/neutronics spatial mesh overlays (mapping schemes in radial axial plane)?*
   One-to-one.
4. *Coupling numerics – explicit, semi-implicit or implicit?*
   Implicit.
5. *Coupling type – external or internal?*
   Internal.
6. *Coupling design – serial integration or parallel processing?*

IV. General

1. *Deviations from the updated Final Specifications?*
   No reflector flux calculations.
2. *User assumptions?*
   None.
3. *Specific features of the codes used?*
   None.

OECD PUBLICATIONS, 2 rue André-Pascal, 75775 PARIS CEDEX 16
Printed in France.